RPE in SD-OCT

12

Andrea Hassenstein and Carsten Grohmann

Introduction

Optical coherence tomography (OCT) was developed in 1991 by Huang, Swanson, and Fujimoto [1, 2]. One of the first OCT prototypes arrived in 1997 in Boston and Hamburg for the first application OCT started with the time-domain technique (TD-OCT) and switched to the faster application of the spectral-domain OCT (SD-OCT) or swept-source OCT (SS-OCT) (Fig. 12.1). The new OCT-angiography (OCT-A) method has been under development since 2015, and provides non-invasive angiography of the retinal and chorioretinal vessels (Fig. 12.1a–f). Since 2001, OCT has been an important component of among macular diagnostic tools due to its capacity for higher resolution and precision.

OCT Technology

OCT offers cross-sectional or tomographic images with micron resolution in eye tissue. The physical basis of OCT imaging depends on the contrast of optical reflectivity between different microstructures of the eye tissue. The light beam is either transmitted, absorbed, or scattered. In most tissue, light scattering outweighs absorption. OCT works in the same way as B-mode ultrasound imaging, except that it uses laser light rather than acoustic waves. The principle of OCT is called low coherence interferometry. The resolution of a typical ultrasound device for eye diagnostics is approximately 150 µm at 10 MHz. A higher resolution of the ultrasound is possible, but attenuates strongly in eye tissue of only 4–5 mm. Therefore, high-resolution ultrasound is limited to the anterior segment of the eye and is not suitable for macular diseases.

OCT is primarily a diagnostic tool for the macula and not for peripheral fundus imaging. Restrictions of OCT are pathologies in the retinal periphery, opacified optical media such as cataract or vitreous hemorrhage, and the absence of fixation. The scanning speed has increased in recent years and therefore OCT images are also now possible in nystagmus patients. Due to its greater wavelengths, OCT images are also available in turbid media. The contralateral eye can be fixed to show the mid-periphery of the fundus. However, imaging of the retinal periphery through the 3-mirror glass is not possible due to the complete backscattering of the light beam.

Time Domain OCT

The first OCT imaging technologies (Time Domain OCT = TD OCT) deliver images

A. Hassenstein (✉) · C. Grohmann
Department of Ophthalmology, University Hospital Hamburg, Hamburg, Germany
e-mail: hassenstein@uke.de; c.grohmann@uke.de

A. K. Klettner, S. Dithmar (eds.), *Retinal Pigment Epithelium in Health and Disease*,
https://doi.org/10.1007/978-3-030-28384-1_12

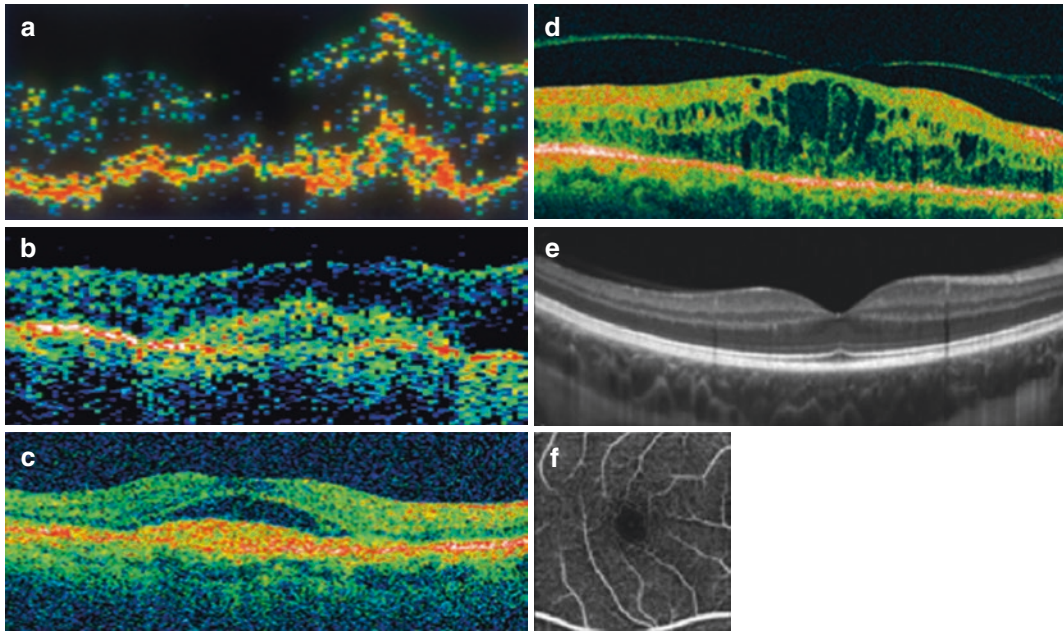

Fig. 12.1 Development of the OCTs from 1997 to 2009 (evolution): OCT started with Time Domain OCT and reached the SD-OCT and SS-OCT generation with improved resolution. Since 2015, OCT angiography has been a new tool for non-invasive angiography through OCT. (**a**) Prototype OCT1, 1997; (**b**) OCT 2, 1998; (**c**) OCT 3 TD Stratus, 2001; (**d**) OCT 4 SD Cirrus, 2007; (**e**) OCT SD, 2009; (**f**) OCT angiography, 2015

with a resolution about ten times higher than conventional ultrasonic B-mode images. The reasons for this are different wave velocities: acoustic wave velocity of 1530 m/s and light wave velocity of 300,000 km/s and different speed of the A-scan application. The resolution of the first TD-OCT components was 10 µm axial and 15 µm transverse. In the next generation of Spectral Domain OCT (SD-OCT), the axial resolution was 3.5 µm.

Ultrasound has a lower resolution of 150 µm but visualizes intransparent structures such as globe boundaries. Due to the light waves, the resolution of the OCT is very high (axial up to 5 µm), but this depends on good transmission (cornea, lens, vitreous hemorrhage).

The light source for the interferometer is a superluminescent laser diode. The interferometer can measure the time delay of optical echoes by comparing the reflected light beam with a reference beam. The reference beam contains a mechanically movable mirror. In TD-OCT, 820 nm wavelength was generally used (1998–2007). The operating wavelength of the SD-OCT probe beam is near infrared (~800 nm), and therefore only minimally visible to the patient. SD-OCT uses either 840 or 870 nm (since 2007) (Table 12.1).

The light from a source is directed onto a partially reflecting mirror and divided into a reference beam and a measuring beam. The measuring beam is reflected by a sample with different time delays.

The light of the sample and the light of the reference mirror are combined and detected. Different reflectivity in the sample leads to different time delays of the reflectivity and leads to a tissue image with reflective properties.

During the generation of TD-OCT, motion artifacts of the eye were also visible due to a longer scanning time through the movable mirror in the reference beam. Patients suffering from poor fixation and lens opacity may not achieve good OCT image quality. In TD generation, TD-OCT can be successfully performed as long as the fundus is visible.

Table 12.1 Overview of the TD OCT, SD-OCT, and SS-OCT and characteristic parameters

	TD-OCT	SD-OCT	SS-OCT
Wavelength	820 nm	840 nm	1050 nm
		870 nm	
Axial resolution	10–20	5	3.5
Transverse resolution	20	15	10
Measurements per A/scan	500	1024	1024
A-scans per B-scan	512	4096	4096
A-scans/s	400	40,000	100,000
Pupil size	4 mm	3 mm	3 mm

The scanning patterns in TD-OCT are radial lines, single or multiple horizontal lines. The macula could never be fully scanned because the areas between the radial lines were interpolated. This was a problem for the interpretation of macular disease, as a pathology could be overlooked due to the absence of a scan position. This problem was solved in the next generation of SD-OCT. The movable mirror in the reference beam is the limiting element which makes TD-OCT unable to provide a higher resolution. The greatest step towards higher resolution was made by SD-OCT by replacing the movable mirror in the reference beam.

Spectral Domain OCT

In contrast to TD-OCT, SD-OCT does not have a mechanically movable mirror in the reference beam, so that significantly higher repetition rates for the A-scan are currently possible (Table 12.1), with more than 40,000 scans per second. An A-scan is generated using an inverse Fourier transformation on the simultaneously acquired data. This results in a higher resolution in axial (currently up to less than 1 μm) and lateral (currently less than 15 μm) direction, with the scan speed also compensating for motion artifacts—which minimizes the likelihood of eye movement during capture, especially in patients with poor fixation. The modern OCT devices have a live eye tracker so that the exact location of the fovea can be guaranteed for follow-up. This was previously a problem for interpretation in TD-OCT.

Another advantage is an improved signal-to-noise ratio by using Fourier transformation of the entire spectrum in SD-OCT and repeated scans for averaging. The spectral interference pattern between the reference beam and the sample beam is dispersed by a spectrometer and collected simultaneously by an array detector. SD-OCT uses either 840 or 870 nm (since 2007). In 840 nm OCT devices, the retinal pigment epithelium (RPE) attenuates the laser beam. This effect increases in RPE thickening/lump formation and drusen and is important for diagnosis.

In addition, SD-OCT generation offers new scanning protocols, i.e. the macular cube protocol of 6 × 6 mm. Here, the entire macular area can be captured with the OCT without missing any pathology. This was made possible by the higher acquisition speed of OCT images and the higher resolution. A high-resolution 5-line horizontal scan is also available depending on the macular pathology.

The difference between TD-OCT (400 scans per second) performed by a mechanical reference mirror and SD-OCT (40,000 scans per second) performed by multiple wavelengths is a factor of 100.

The advantages of higher resolution, scanning speed and macular cube led to the integration of OCT as the macular diagnostic standard specifically for age-related macular degeneration (AMD) and other macular diseases.

Swept Source OCT

In OCT scanning with swept source (SS-OCT, optical frequency range), the light source is rapidly swept in wavelength and the spectral interference pattern is captured on a single or small number of receivers as a function of time. Higher

scanning speeds enable denser scanning and better registration. The swept source OCT also has a lower depth sensitivity, which allows better visualization of structures in the depth of the retina. The reason for this is that SS-OCT has a longer wavelength (infrared) than SD-OCT, so there may be less scattering of optical opacity (i.e. lens or vitreous exchange) and the imaging of deeper retinal structures has fewer signal-to-noise patterns. Faster acquisition speeds also mean a higher scanning density of the macula, minimizing the risk of missing pathology and enabling three-dimensional OCT scans (100,000 A-scans per second). The SS-OCT (1050 nm) offers slightly better penetration of the RPE and thus better visualization of the underlying choroid (enhanced depth imaging). The invisible infrared laser does not distract the patient during the scan (Table 12.1).

OCT Angiography

High-resolution OCT images and fast image acquisition led to the development of OCT angiography. The presentation of OCT images in the z-axis (en-face visualization) became increasingly important in SD-OCT generation. This technique enabled the en-face visualization of retinal and choroidal vascular supply by OCT.

The current gold standard for the diagnosis of vascular diseases of the retina or choroid vessels is fluorescence angiography (FLA) or ICG angiography (ICG). However, other diagnostic methods have been developed for significant contraindications (renal dysfunction in the FLA or hyperthyroidism on ICG allergies).

Rapidly repeated OCT scans track the movement of intravascular corpuscular parts of the blood and subtract it from the static topographic OCT image. This allows the detection of blood vessels and the monitoring of blood flow without invasive methods such as digital subtraction angiography (DSA for cardiovascular imaging).

The common SD-OCT is usually used in two dimensions and mainly as tomography. Nevertheless, 3D animation is possible in the viewer of the devices. In OCT-A, B-scans are used en-face and a three-dimensional image is created. If the blood flow is slower than the time between the B-scans of the OCT device, the OCTA interprets this as a lack of blood flow and no vascular system becomes visible. Therefore, OCT-A does not detect any leakage or blockage. This is important for the interpretation of OCT-A images. With the 3 × 3 mm retinal scan cube, the images are high-resolution, and they are of poorer quality in larger cubes (6 × 6 mm).

The lowest flow velocity detectable with OCT-A is called the "slowest detectable flow (SDF)". This depends on the interscan time of the OCT-A device. OCT-A devices with slow intermediate scan speed detect slower flow rates.

The most common four layers of retinal vascular structures are represented by the OCT-A: The superficial retinal plexus, the deep retinal plexus, the outer retinal layer and the choriocapillaris. Neovascularizations penetrating the RPE can be visualized with this technology. Today (2019) there is a common nomenclature, but due to different algorithms and visualization possibilities a comparison between images of different providers is still a challenge. The OCT-A can be performed with SD-OCT or SS-OCT technology. The axial resolution for small capillaries is less than 5 µm and laterally less than 15 µm. Infrared lasers that are not visible to the patient are usually used. Due to the longer scanning times, eye tracking and averaging technologies are used. The main problem with OCT-A is the different standards of the layers in the different devices. A comparison between OCT-A devices is not possible.

SD-OCT and RPE Absorption Spectrum

The laser light of the OCT (central wavelengths, e.g. 840 nm) reaches the melanin of the RPE where absorption takes place. In the laser beam, three pigments are highlighted, which lead to absorption—and thus to an impairment of image resolution: The hemoglobin in the blood vessels (especially in visible light absorbing yellow/green and especially blue, Fig. 12.2), the xan-

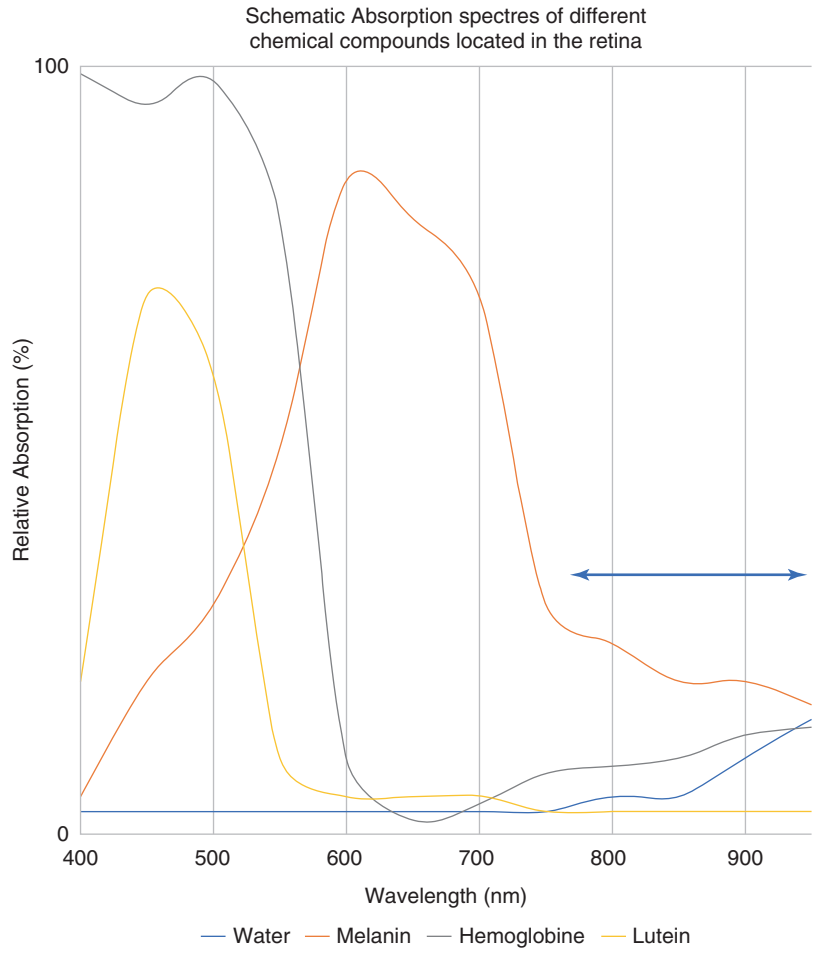

Fig. 12.2 Schematic absorption of light from melanin, lutein, hemoglobin and water depending on different wavelengths. The blue line with two arrows marks the optical window for OCT imaging. It is also clearly visible that lutein absorbs at shorter wavelengths (like "natural sunglasses")

thophyll and lutein in the macula lutea region (absorption maxima in the blue spectral range, "natural sunglasses", Fig. 12.2) and the melanin of the RPE (visible light, 400–1400 nm) [3, 4]. With increasing wavelength, the absorption of the retinal pigment epithelium decreases, so that OCT lasers with a higher wavelength are more advantageous for the visualization of pathologies in the RPE and sub-RPE structures (Fig. 12.2). The best optical window for SD-OCT imaging of the macula is therefore in the near infrared range from a wavelength of approx. 800 nm (Fig. 12.2).

Indocyanine green (ICG) is used for the fluorescence angiographic examination of choroidal pathologies. The emission and absorption spectrum of tissue is solvent-dependent and lies in the optically transparent range of the RPE (fluorescence maximum around 800 nm). Fluorescein, on the other hand, has its emission maxima at about 510 nm, so that it cannot be used as a means of imaging sub-RPE structures. An exception are pathologies without RPE, i.e. geographic atrophy or RPE rips [5].

Scan Pattern

TD-OCT began with radial scans consisting of 6–12 high-resolution line scans passing through the macula. The disadvantage of radial scanning is that the device interpolates between scans. The TD-OCT scan patterns were not suitable for the follow-up of wet AMD. The risk of overlooking an intraretinal cyst was too high without the macular cube.

In SD-OCT generation (and SS-OCT), the macular cube scan and various line scans are most common. The macular cube scan consists of a square area of 6 × 6 mm centered on the fovea. The scans are usually of relatively lower resolution due to time gain. Raster scanning is the technique used to obtain cube scans of the macula. Other scanning protocols improve the size of the scanned area.

In order to scan the entire macula, a cube scan is essential, especially for the detection of fluid in wet age-related macular degeneration (AMD). The highest resolution is achieved with three or five high-resolution linear scans. For the follow-up of macular pathologies, it is very important that the devices can reliably scan the same position for each examination. The same OCT device should always be used for tracking, as the software of different devices defines different reference lines for segmentation. The macular cube scan is probably the safest way to ensure that no pathologies are overlooked. Although the scanning protocols of different manufacturers differ, the standard protocol is a 6 mm macular cube [6–8].

It is very important to define the segmentation lines in OCT-A to make diseases and research comparable. Segmentation lines for automated segmentation must be clearly distinguishable: "for the RPE-Bruch's membrane (BM) complex), the highly reflective edges of the ellipsoid zone and the RPE-BM complex are suitable [9]".

With DICOM import and export as the target, registration and tracking by various devices and vendors will be possible. Eye tracking is established in SD-OCT generation. Tracking should only be performed with the same device. With the OCT-A, the standard level descriptions between the devices are different, therefore standardization is very difficult.

Interpretation of the OCT

Qualitative Assessment

The qualitative interpretation of OCT images in macular diseases is clinically more important than quantitative evaluation. Typical qualitative diagnostics using OCT are macular holes and epiretinal membranes as well as cystoid macular edema.

Linear scans with high resolution are used for the interpretation of RPE. For control examinations of e.g. wet AMD, it is absolutely necessary to scroll through the entire macular cube. It is not sufficient to interpret only one high-resolution scan for one treatment indication. The RPE and the choriocapillaris are difficult to distinguish due to the similar reflection pattern. The RPE layers can be clearly distinguished by the higher resolution of SD-OCT (Fig. 12.3). The RPE layer is highly reflective and leads to a backscattering of the light beam of the OCT (shading of the light beam below the RPE). The atrophy of the highly reflective RPE leads to a reverse shadowing [10–12].

The most important for perfect visualization of individual retinal layers is the different reflectivity of the merging structures, e.g. in the retinal nerve fiber layer (high reflectivity) and in the vitreous body (no reflectivity).

Figure 12.3 shows a detailed description of each retinal layer in SD-OCT. The outer segments of the photoreceptor contact the RPE located on the BM as a single cubic layer. Below the BM, the choriocapillaris and the larger choroid vessels appear in the OCT.

The high-resolution SD-OCT image increasingly resembles a histological tomogram. For the interpretation of OCT images, however, it is important to note that OCT is still an image of reflectivity and not a true histology. Therefore, OCT may show several reflectivity lines of a cell structure such as the photoreceptors (outer segments and the connection to the inner segments), but also vice versa. In Best's disease, highly reflective deposits within the outer retina simulate a lack of highly reflective photoreceptors and RPE, although they are present but not visible to the light beam.

Quantitative Assessment

Quantitative evaluation is particularly helpful for the measurement of the optic disc and the retinal nerve fiber layer (RNFL) for glaucoma diagnostics. The thickness of macular edema can be easily measured using topographic maps. Quantitative

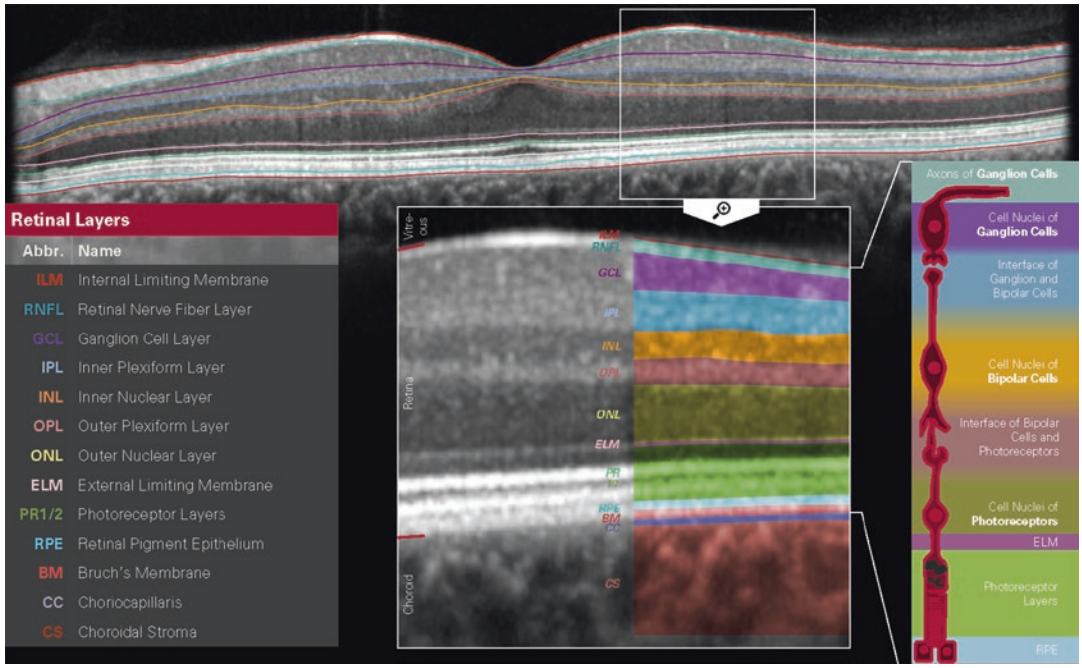

Fig. 12.3 A detailed colored representation of each layer of the retina in SD-OCT (image courtesy of Heidelberg Engineering GmbH, Heidelberg)

OCT interpretation is based on the OCT device's ability to distinguish between different retinal layers with different reflectivities, which requires specific segmentation. The RPE is a very important baseline for manual and automated segmentation together with the retinal nerve fiber layer.

OCT Characteristics of RPE and Bruch's membrane (BM)

Modern SD-OCT has enabled a deeper understanding of RPE and its function in pathology. The RPE and the underlying Bruch's membrane (BM), which can be considered as a coherent region, have an average thickness of about 18–25 µm. BM represents a boundary between the choroid and the RPE. Histologically, it is surrounded by the basement membranes of the choroid vessels on one side and the RPE cells on the other. It consists of elastic fibers and collagens. The retinal pigment epithelium is histologically cubic with nuclei that are essentially close to BM. On the apical side, RPE cells are filled with melanin granules, numerous mitochondria and lipofuscin. Due to the limited light penetration beyond the pigmented RPE and the decay of the OCT signal with depth by absorption and scattering, the image at the choroidal level shows a significantly lower resolution [13].

In SD-OCT, the contiguous region of RPE and BM is the outermost highly reflective continuous line (Fig. 12.4). RPE/BM thickness in normal eyes correlates positively with age. The thickness of the RPE/BM complex is significantly greater in dry AMD compared to age-appropriate controls.

The SD-OCT image visualizes four hyperreflective lines within the outer retina in a healthy macula (Fig. 12.4). When interpreting a macular scan, all four lines should be identified, provided the image quality is high enough. Of the four lines of the RPE complex, the innermost fine line is the external limiting membrane (ELM), followed by the ellipsoid zone (inner and outer photoreceptor connecting line) and the outer photoreceptor segments (interdigitation line) and the RPE. Beyond the BM are the choriocapillaris and choroid.

Alterations of the RPE/BM complex in retinal diseases can occur as a result of increased detachment (Fig. 12.5), atrophy, tear or thickening of the RPE.

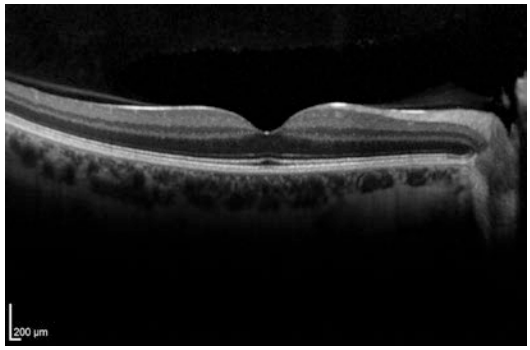

Fig. 12.4 In SD-OCT, four different highly reflective lines can be distinguished in the outer retinal segment. The innermost line is the external limiting membrane (ELM), followed by the inner segments of the cones (connecting line of the inner and outer segment zone), the outer segment line of the cones (interdigitation line) and the outermost segment line of the RPE

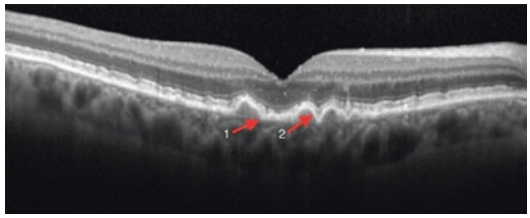

Fig. 12.5 SD-OCT of serous Drusen. The Bruch' membrane (BM) (arrow 1, horizontal fine line) and RPE (arrow 2, highly reflective line of RPE detachment) can be represented as two separate structures

Systematic Verification of RPE Pathologies in SD-OCT

RPE Detachments

The RPE/BM complex in retinal diseases can occur with increased detachment. A pigment epithelial detachment (PED) is an elevation of the RPE from BM with a size of >400 µm width and >75 µm height or >200 µm height. The underlying reflectivity can be divided into homogeneous hypo-reflectivity, hyper-reflectivity and heterogeneous reflectivity. In serous RPE detachment, the RPE is detached and the layer below the RPE is optically empty or only slightly reflective (Fig. 12.6). In an optically empty serous PED, the underlying BM is visible, but not always in crystalline deposits within the detachment cavity (Fig. 12.8).

Serous RPE Detachment (sPED)

In serous RPE detachment, the liquid in the sub-RPE space is optically empty (Fig. 12.6). The separated cavity is surrounded by RPE on one side and BM on the other side. The sPED must be scanned from the macular cube to ensure that the PED is fully serous and no fibrovascular neovascularization can be found.

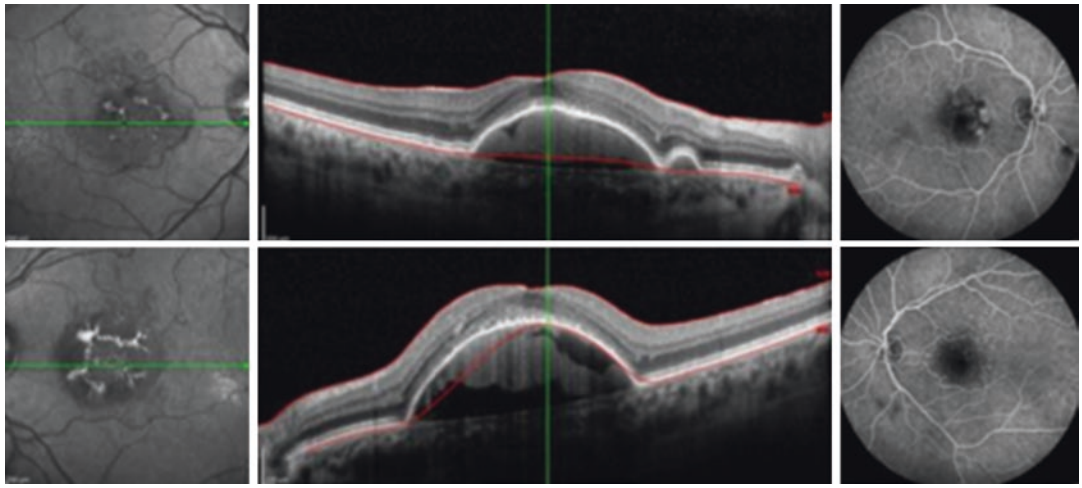

Fig. 12.6 69-year-old patient with VA 0.4, no MMP's (metamorphopsia). Left: Infrared image shows RPE pathologies in butterfly form. Middle (OCT): optically empty area under the RPE (slightly reflective) and attached sensory retina. Right: FLA of the left eye without leakage or staining, of the right eye with staining and no leakage

SD-OCT showed a typical serous PED and slightly constant hyperfluorescence in FLA, but no evidence of choroidal neovascularization (CNV). Treatment was not necessary because no neovascular process was identified in OCT and FLA (no leakage) (Fig. 12.6).

In case of intraretinal cystoid formation and sensory detachment in sPED, a neovascular process must be suspected (Fig. 12.7a, b). In OCT scans, a neovascular highly reflective process or retinal angiomatous proliferation (RAP) lesion must be sought. FLA/OCT-A should be used to identify CNV (type 1 in conjunction with PED). Anti-VEGF treatment has been initiated.

After anti-VEGF treatment (after 3 months), VA (visual acuity) improved to 0.2 and anatomical improvement was achieved. Secondary focal RPE atrophy instead of detachment occurred in OCT after treatment (Fig. 12.7b).

In long-lasting serous PED, the sub-RPE fluid may indicate crystalline deposits (Fig. 12.8). The fluid begins to become turbid after many years of serous RPE detachment.

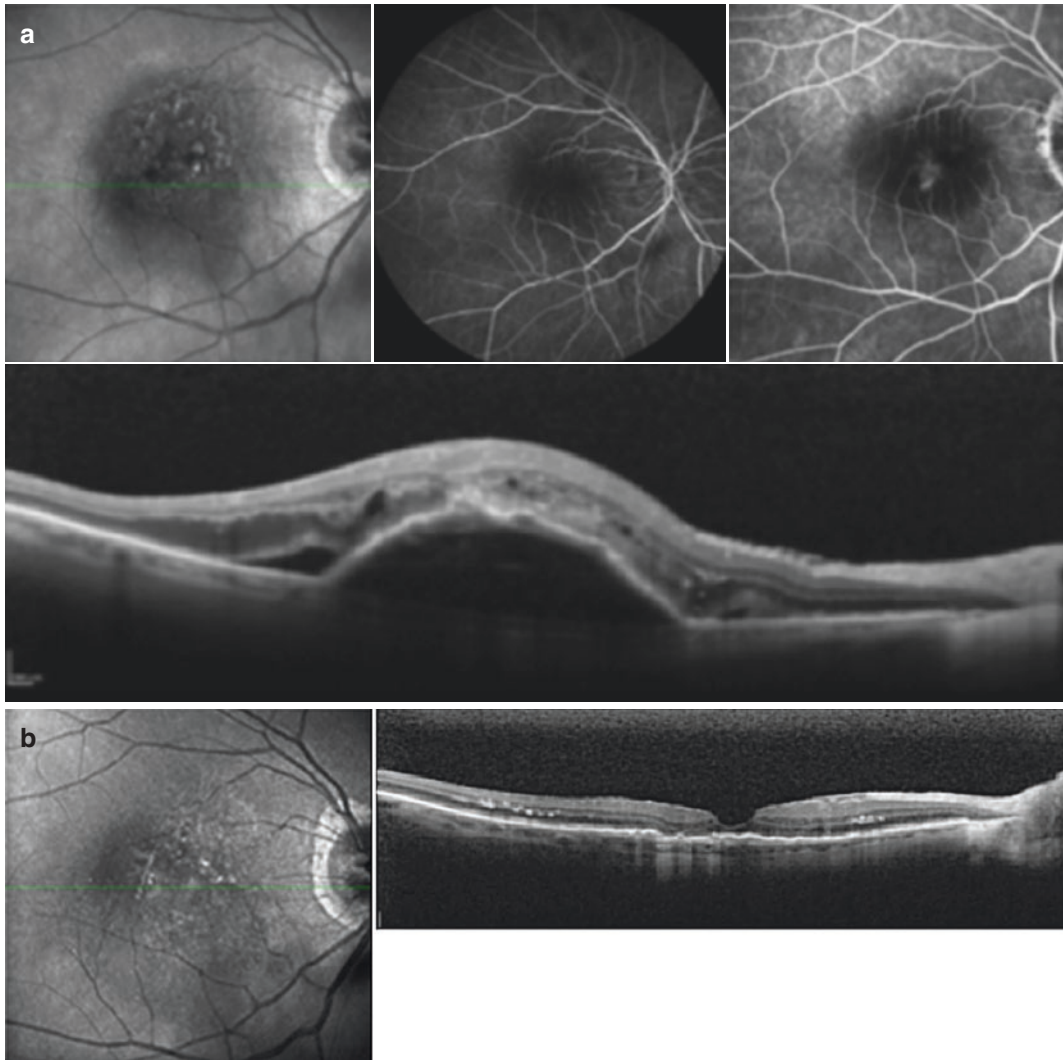

Fig. 12.7 (**a**) 75-year-old patient with VA 0.1. sPED is detected in OCT and sensory detachment and intraretinal cystoid formation. In FLA a leakage in the fovea is detectable and a choroidal neovascularization is suspicious due to the fine leakage. No RAP lesion could be verified in OCT. (**b**) Left: Infrared image after intravitreal treatment, right: OCT shows a subnormal foveal configuration and a focal RPE atrophy with increased light reflection into the choroid

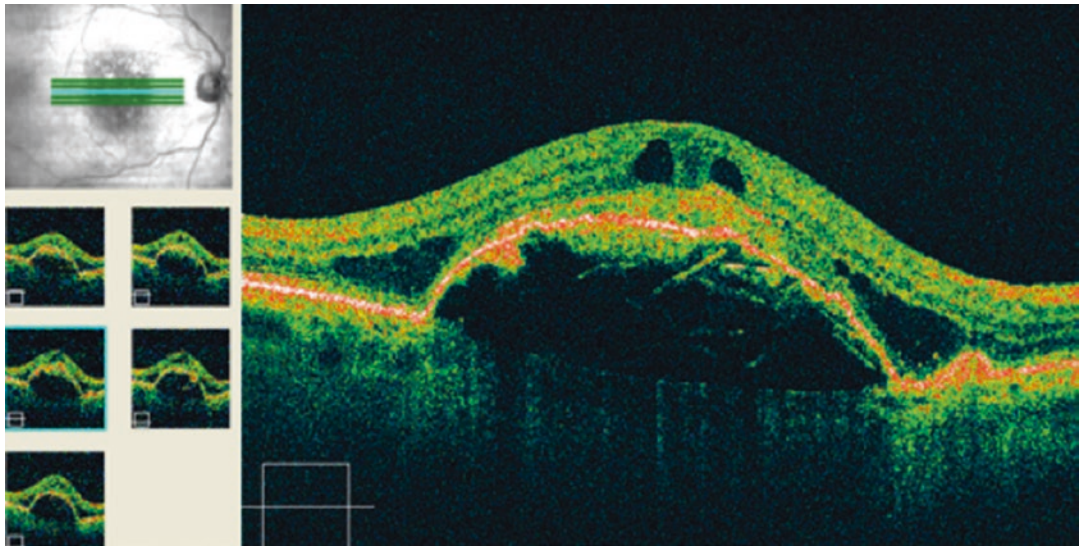

Fig. 12.8 SD-OCT shows crystalline deposits in the sub-RPE cavity as in the long-term RPE detachment. Remarkable is the intraretinal cystoid formation and the sensory detachment, which is rather an intraretinal schisis

Hyperreflective intraretinal and subretinal foci, as seen on SD-OCT, correlated with RPE cells in histology and with funduscopic hyperpigmentation. Any loss or dissociation of RPE leads to hypertransmission of light below the RPE. In histology, the subretinal hyperreflective vitelliform material corresponded to apically expelled RPE organelles and outer segment debris. The occurrence of intraretinal hyperreflective foci was preceded by a thickening of the RPE-BM complex. Over time, the hyperreflective foci of the RPE-BM complex migrate into the retina. Hyperreflective foci in the PED can be quantified and subsequently followed by serial SD-OCT [14]. This RPE foci migration precedes the RPE atrophy detected by the OCT [15].

Fibrovascular RPE Detachment (fPED)

In the event of fibrovascular detachment of the RPE, the space under the RPE is turbid and medium to highly reflective (Fig. 12.9). Depending on the reflectivity of the RPE and the sub-RPE structures, the BM may not be visible. In fPED, always search for RAP lesions or CNV (PNV = pachychoroid CNV) through FLA or OCT-A. In rare cases, ICG is mandatory to detect choroidal polypoidal vasculopathy (PCV) because treatment would be different (anti-VEGF versus photodynamic treatment (PDT)).

Choroidal Polypoidal Vasculopathy (PCV)

In ICG, the PCV is identified by polyps of the choroidal vessels near the optic disc. In OCT

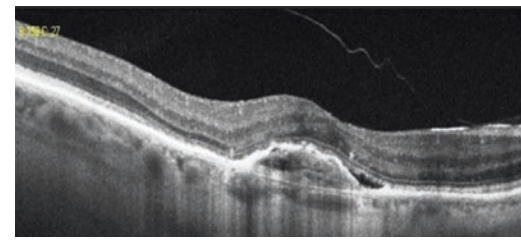

Fig. 12.9 The highly reflective layer of the RPE forms a convex line and the sub-RPE lumen is medium reflective. In addition, there is a sensory detachment laterally to the fovea

the PCV can be visualized by several PED's and medium to highly reflective fibrovascular structures below the RPE. In addition, subretinal hemorrhage often occurs and hard exudates are typical. The hemorrhage often hides the PED finding on the OCT.

In PCV, SD-OCT shows sharp tips and multiple pigment epithelial detachments. This helps in the differentiation from occult CNV's.

The distinction in SD-OCT between PCV and occult CNV shows typical indicators: sharp pigment epithelial detachments, tomographic notch, hyporeflective lumen of the PED, several PED's and hard exudates (funduscopy). These OCT signs occur much more frequently in PCV than in occult CNV. PCV shows lipid and hemorrhage through the polyps and the choroid is typically thickened, changes in RPE are visible and no drusen are visible. SD-OCT detects the vascular lesions of PCV in the sub-RPE space.

This suggests that PCV may be a type 1 CNV variant [15].

The PCV does not respond properly to anti-VEGF treatment. Therefore, it is important to identify PCV in cases of poor response to anti-VEGF and perform ICG in these cases [16]. The treatment differs for occult CNV (type 1) and PCV—therefore, identification is important.

RPE Rip

A possible complication of neovascular AMD (nAMD) may be RPE rip, in which the RPE is torn and leads to a fibrotic scar of the macula (Figs. 12.10 and 12.11b, c). VA decreases as the scar increases. The development process can be

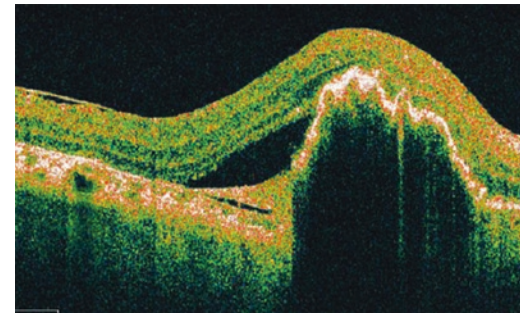

Fig. 12.10 The RPE rip demonstrates an interruption of the RPE layer. The elastic RPE layer shows bundling and a wavy appearance (like a rubber band). A subretinal detachment by the traction of the RPE elevation is typical. The loss of RPE in the RPE rip is associated with inverse shading

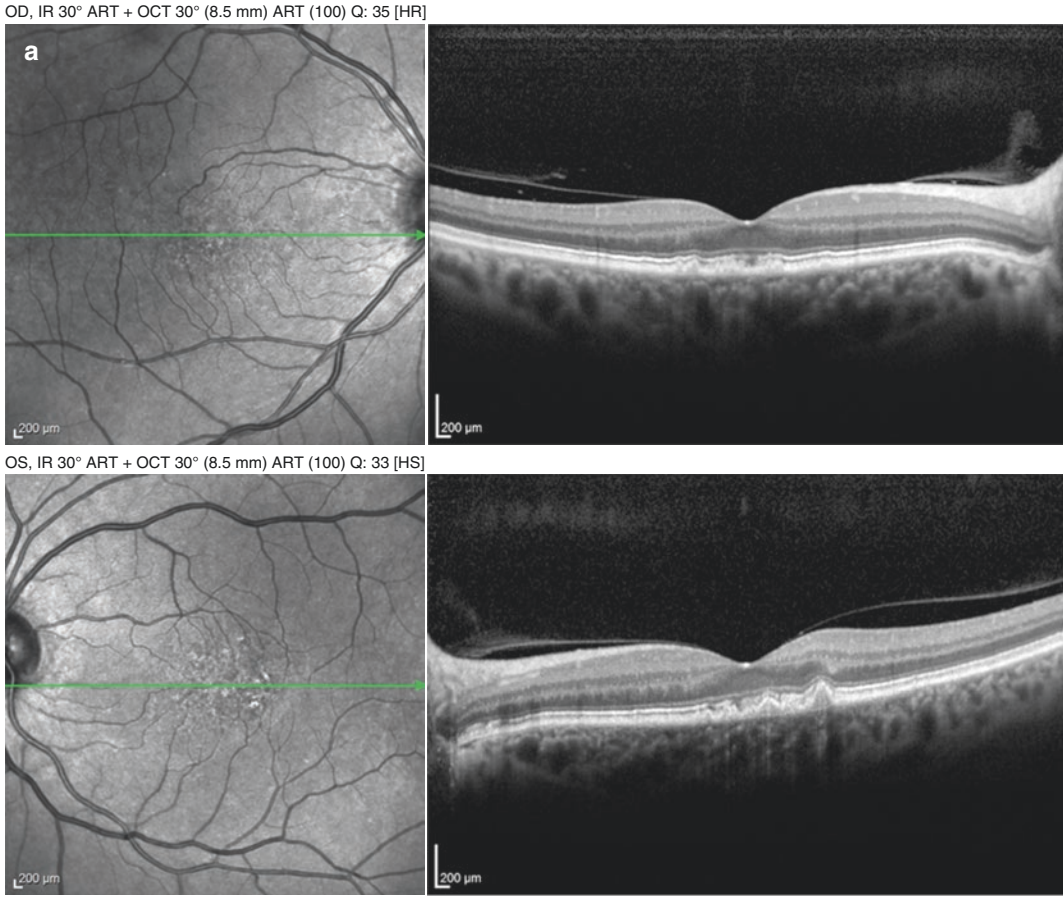

Fig. 12.11 4 years follow-up of a development of RPE rip, from drusen to sPED, RPE rip and subsequent CNV (Type 1). (**a**) SD-OCT shows small miliar, spiky drusen. (**b**) Both eyes developed a sPED, with an RPE rip on the left eye, OCT. (**c**) Increasing scarring and sensory detachment of the rupture side (OS) can be observed in OCT. (**d**) A macular scar in OCT and new intraretinal cystoid formation as an indicator for CNV are found

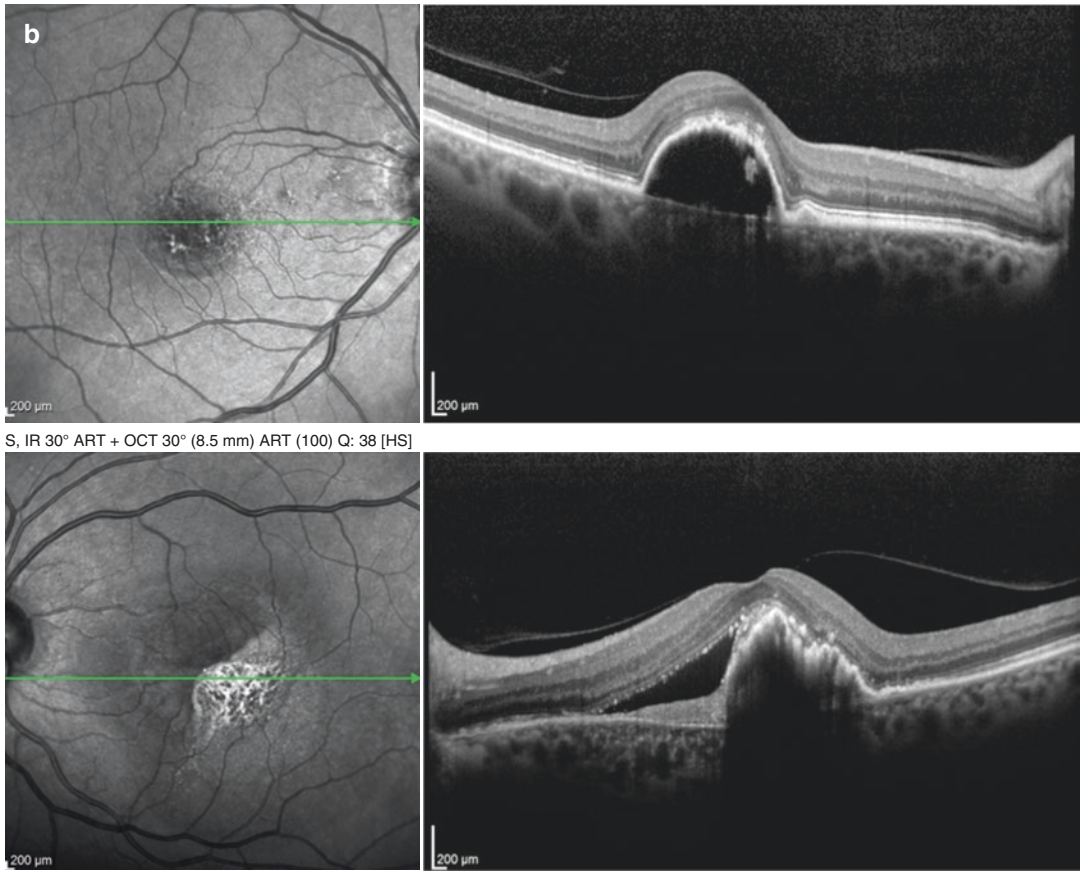

Fig. 12.11 (continued)

observed with modern OCT. In the event of a tear of the PED (rip), the elastic RPE rolls up like a rubber band. The torn part shows atrophy of the RPE with inverse shading of the OCT light beam.

The RPE Rip is most common in an underlying choroidal neovascular process. In the case of an active CNV base, anti-VEGF treatment must be applied and continued. Vascularized PED tears are mainly associated with occult CNV, PCV and RAP lesions.

The follow-up of a patient from 2014 to 2018 with some drusen at the beginning (VA 0.3) and finally an RPE rip and fibrotic scar in 2018 is shown in Fig. 12.11 (VA 0.05) (Fig. 12.11a–d).

Central Serous Chorioretinopathy (CSCR)

Typical OCT findings in CSCR are neurosensory detachment (optically empty subretinal fluid) between the outer retina and the RPE layer and focal serous (s) PED, either as a focus or double detachment (Fig. 12.12a, b). In the acute stage, the focus sPED can often be identified (75%). In rare cases, a double peak sPED is visible. In chronic stages of CSCR RPE, atrophy and loss of photoreceptors

Fig. 12.11 (continued)

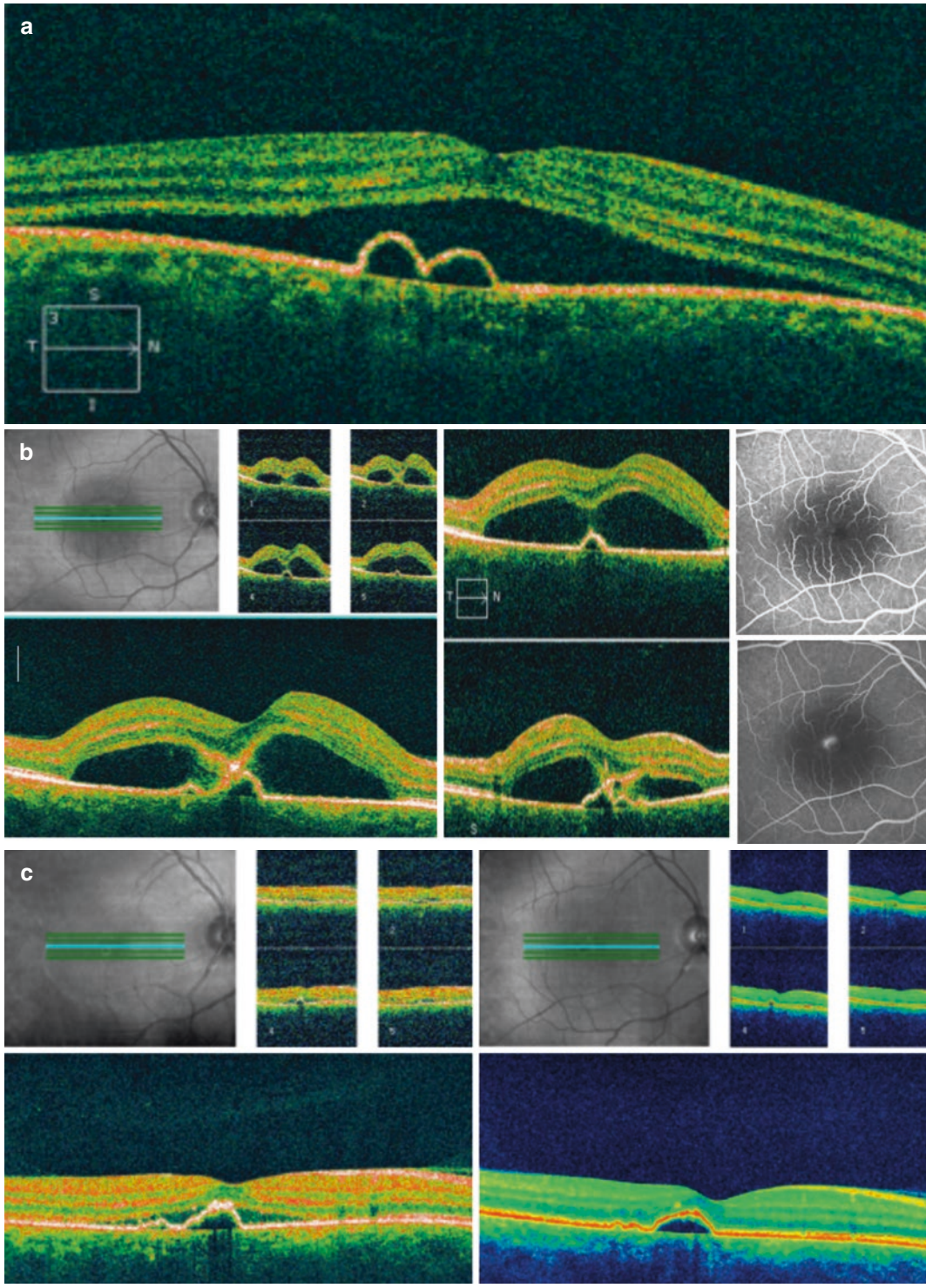

Fig. 12.12 (**a**) OCT in CSCR shows a double peak serous PED and an accompanying sensory retinal detachment. VA is 0.5 OD. Right: FLA shows the typical leakage very close to the fovea (smoke banner phenomenon). (**b**) Left: OCT image shows a sensory detachment and a rare scarring of the retina with the underlying sPED. Right: FLA shows typical subfoveal smoke banner phenomenon, not suitable for laser treatment of sPED (leakage = source point). (**c**) One month later the sensory detachment has resolved, and the VA has improved to 1.0. The sPED remains and may exhibit recurrent CSCR in the future

may occur. CSCR is defined by subretinal fluid and high choroidal permeability on the OCT. The FLA shows a chimney smoke-like pattern and an umbrella leak (Fig. 12.12). The exemplary patient depicted in Fig. 12.12 suffered from visual deterioration in CSCR (VA 0.8). OCT shows sensory detachment and scarring of the sensory retina and the underlying RPE separation in CSCR (rare case). FLA shows sub to juxtafoveal leakage. After treatment, the sensory retina was attached (Fig. 12.12c).

In OCT-A of the superficial and deep retinal plexus, the outer retina and the choriocapillaris showed no altered flow pattern correlating with the leakage point in CSCR [17].

Drusen

Typical signs of early AMD are drusen and atrophy of RPE, in late-stage geographic atrophy and wet AMD. Late AMD exists in dry (85%) and wet (15%) form. In addition to classic late AMD, the lesion shows retinal angiomatous proliferation (RAP) and PCV. Pathological characteristics of AMD are an accumulation of lipofuscin within RPE cells and the appearance of drusen.

The clinical classification of AMD is divided into small drusen (<63 μm), medium drusen (>63 to <125 μm) and large drusen (>125 μm). Small drusen are only droplets and represent normal aging changes. Medium drusen show the early stage of AMD, large drusen the medium AMD including pigmentary changes. Late AMD is defined as neovascular AMD (nAMD) and/or geographic atrophy (GA) [14].

In general, drusen are accumulations of extracellular material and metabolites between BM and RPE (e.g. lipofuscin, cholesterol). The material in SD-OCT has a medium to highly reflective and largely homogeneous form. Drusen can occur as single drusen or in confluent distribution. In addition, the overlying structure may show hyperreflective lesions.

In AMD (dAMD and nAMD), both hard and soft drusen types may occur.

Reticular Drusen (Hard Drusen)

Reticular drusen are granular, irregular and hyperreflexive lesions above the RPE. Hard/reticular drusen show sharp hyperreflexive peaks in OCT compared to flat curved RPE detachments in soft drusen (Figs. 12.5, 12.11a, 12.13, and 12.14) [18, 19].

Soft Drusen

In the early phase, an expansion of the joint structure of BM and RPE in the OCT can be observed. Basal laminar drusen are probably an early form of serous drusen and differ in sub-RPE thickening in SD-OCT (BM can be distinguished from RPE). Soft drusen are identified on OCT by discrete elevations of the RPE layer at the BM level. Soft drusen are typically considered as a collection of optically scattering material (Figs. 12.5 and 12.14) between RPE and BM. In larger drusen or drusenoid PEDs, a greater height of the RPE occurs, often dome-shaped, with hypo- or medium-reflective material separating the RPE from the underlying BM [8, 20].

SD-OCT identifies different types of sub-RPE hyperreflectivity in the regression of calcified drusen.

Type 1 is a multilaminar hyperreflection from the suspected inner part of the BM, type 2 is also a multilaminar hyperreflection from the outer part of the BM and type 3 is a multilaminar fragmented hyperreflection from both parts of the BM. Drusenoid material not removed by macrophages develops calcification (hyperreflection) similar to the arteriosclerosis process. The deposits of lipids and cholesterol, if not removed by macrophages, will likely follow calcification of lipids (hyperreflection in the sub-RPE layer) [21].

Reticular Pseudodrusen

SD-OCT helped to identify so-called reticular pseudodrusen. Reticular pseudodrusen correspond to discrete collections of hyper-reflective material located above the RPE between the RPE and the ellipsoidal zone. Pseudodrusen are hyperreflective granule structures in SD-OCT [8, 20, 22, 23]. The Beaver Dam Eye Study identified reticular drusen as one of the major risk factors for the development of advanced AMD.

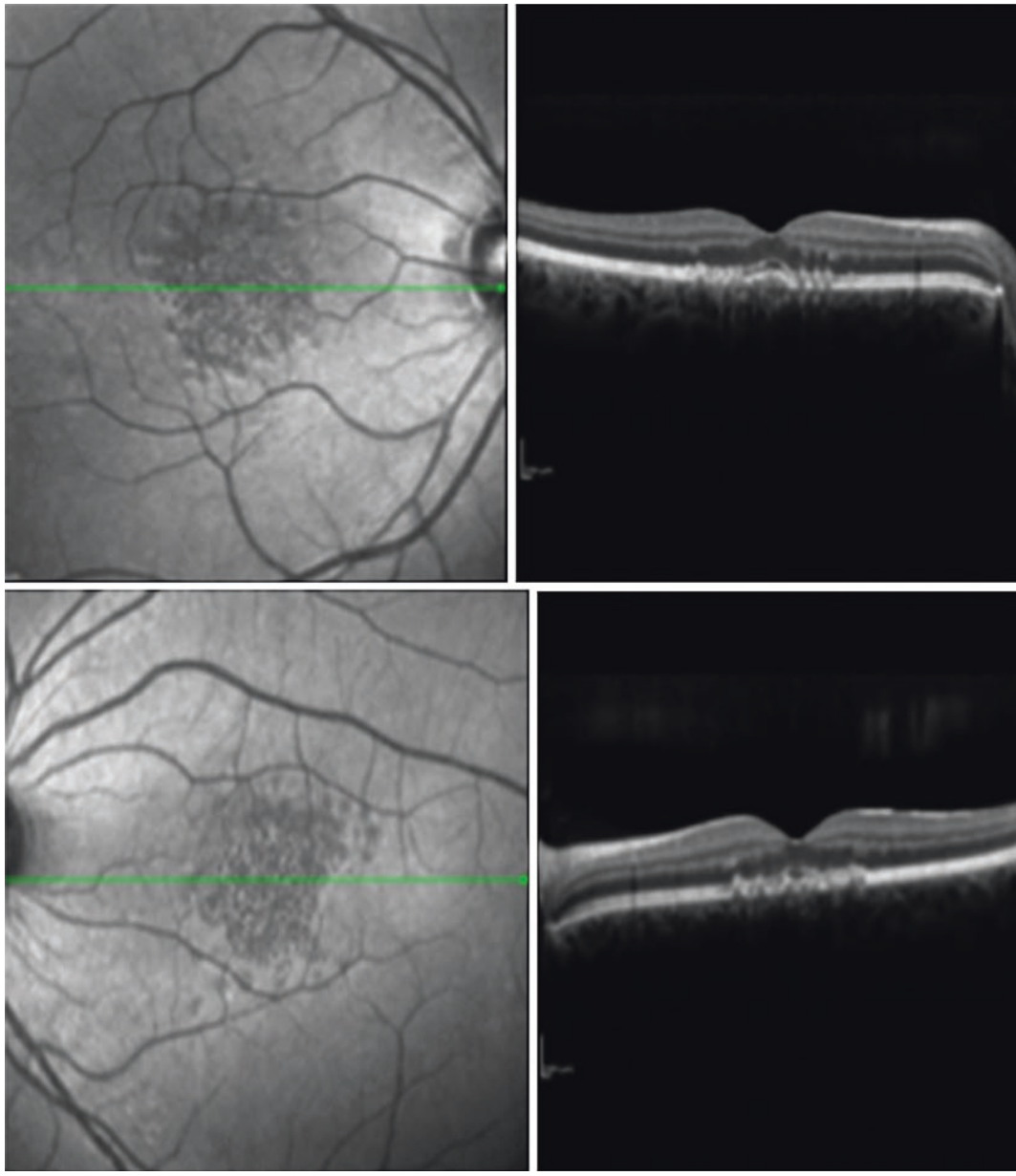

Fig. 12.13 OCT Spectralis demonstrates miliar drusen and VA 1.0 (29-year-old male)

RPE Thickening

RPE Thickening by Neovascularization

Age-Related CNV (nAMD)

The typical finding of OCT in nAMD is fibrovascular RPE thickening and subretinal fluid or cystoid macular edema. Subretinal hemorrhage may also occur. The classification of CNV into classic and occult CNV is based on FLA. But in high-resolution OCT, differentiation can usually also be accomplished.

Classic CNV (type 2) penetrates the RPE/BM complex and is in the subretinal space between

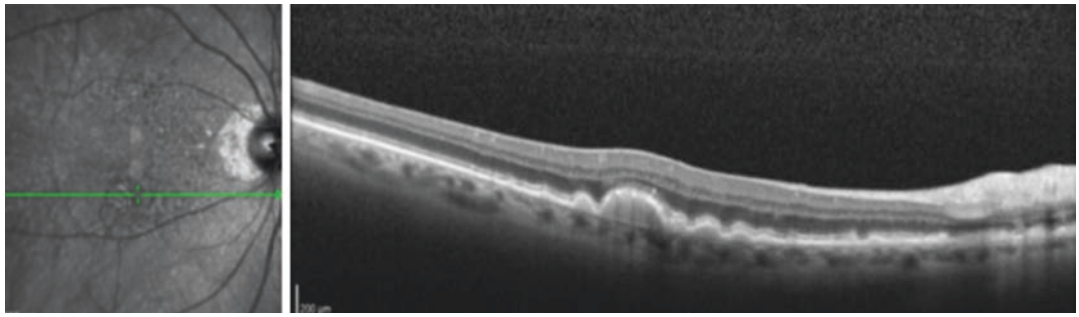

Fig. 12.14 A typical image in serous drusen at early AMD with VA of 1.0. The Spectralis OCT shows a typical curvy RPE separation with a central reflection zone beyond the RPE. The BM is visible as a fine horizontal line beyond the deposition. The drusen show different size and extension

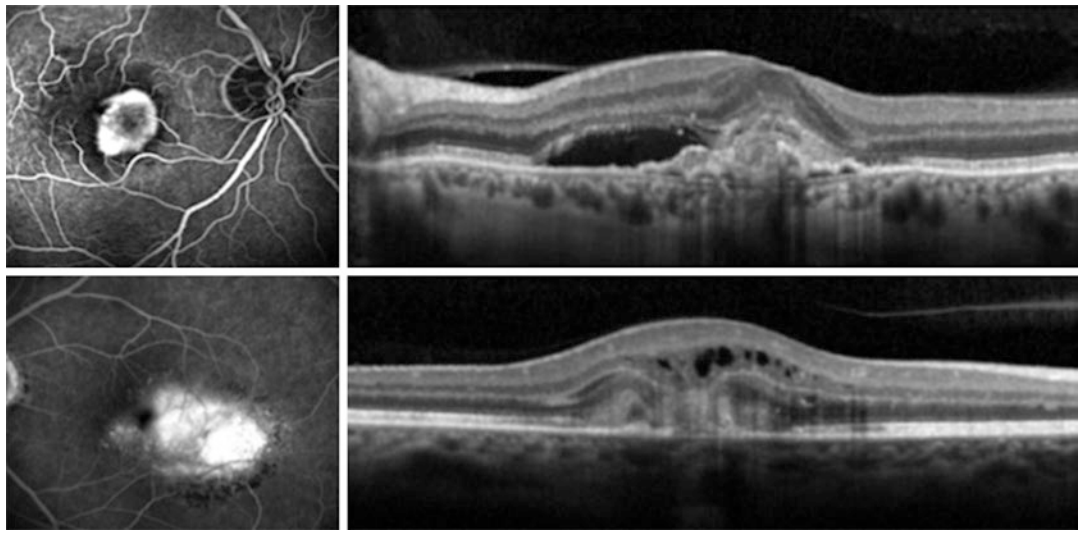

Fig. 12.15 Above: FLA with a typical classic CNV (type 2), sharply defined and above the RPE. OCT (Spectralis) on the right shows the thickening of the RPE/BM layer complex (= neovascular membrane) and subretinal fluid. Below: FLA with occult CNV (type 1), diffuse leakage. OCT shows thickening of the RPE/BM complex and typical intraretinal cystoid formation

the RPE and sensory retina. In FLA, type 2 is well delimited by the visualization of the pathological new subretinal vessels of the macula (Fig. 12.15).

In contrast, the occult CNV (type 1) is the neovascular tissue below the RPE (between RPE and choriocapillaris). In these cases (type 1), the frequency of intraretinal cystoid edema is significantly higher than in classical CNV (type 2). Subretinal fluid is more abundant in classical CNV (Fig. 12.15).

Mixed forms of both types 1 and 2 are common in nAMD. OCT is very important for fluid detection in each retinal and subretinal space and leads to further treatment with anti-VEGF. The indication for the treatment of age-related CNV is based on any fluid within the retina (cystoid spaces or subretinal fluid) regardless of the layer [22, 24, 25].

Type 1 CNV represents the occult CNV (in FLA), which originates from the choriocapillaris. It is often associated with an overlying PED. OCT-A in type 1 CNV shows an entangled network of fine vessels or a round tuft of small-caliber capillaries.

Type 2 CNV corresponds to the classic CNV in FLA (incidence 9–17%). The CNV is located above the RPE in the subretinal space. In the OCT-A, the macula above the RPE presents high flow vessels, which are described as medusa- or glomerulus-shaped patterns.

Type 3 CNV combines type 1 and type 2 patterns. It is previously referred to as RAP lesion or occult chorioretinal anastomosis. Type 3 is predominantly perpendicular to the retinal layers and may extend to the RPE.

OCT-A was compared with multimodal imaging (FLA, ICG, SD-OCT) for the need for treatment in wet AMD. Five results in OCTA were described: (1) form of neovascular lesion, (2) branching patterns (fine or large vessels), (3) anastomoses and vessel loops, (4) peripheral arcade or dense vessel endings, (5) perilesional hypointense halo. Three or more of the criteria represent an active lesion and have been treated with intravitreal injection and two or fewer criteria show an inactive lesion without subsequent treatment. This criterion division corresponds to 95% of the treatment indication by conventional multimodal imaging (FLA, ICG, SD-OCT).

Different types of CNV in exudative AMD can be visualized and differentiated with OCT-A. Type 1 CNV were larger with little differentiation from the surrounding vascular system and were visible on the slab "Mid-Choroid", "CC" and "RPE". In contrast, type 2 CNV showed a sharp demarcation from the surrounding vascular structure reaching to the slab "outer retina" [26]. The use of ICG shows a larger size of CNV compared to different OCT-A devices with different wavelengths, scan patterns and algorithms. Due to different segmented layers for the evaluation of CNV quantitative parameters such as CNV range, vessel density recommends a standardized OCT-A protocol for analysis [27]. OCT-A was generally less successful in detecting CNV compared to ICG. OCT was superior in the detection of CNV type 1 compared to type 2. SD-OCT-A is limited by the detection of blood flow velocity, rather than lesion type [28].

Myopic CNV

Myopic CNV is similar to age-related CNV in OCT. OCT shows similar results in highly myopic CNV. The myopic CNV is typically found as classic CNV (type 2) above the RPE and shows little edema or fluid (very rare intraretinal cysts).

Pachychoroid CNV (PNV)

Pachychoroidal diseases are considered disorders of the RPE and a typical choroidal thickening. Identification of pachychoroidal diseases began in 2013 due to long-wave SS-OCT (EDI enhanced depth imaging) and faster scan acquisition.

Pachychoroidal diseases show an increased choroidal thickness, dilated veins in the Haller layer (pachy veins) and dilution in the Sattler and Choriocapillaris layer.

The choroidal thickness is between 220 and 350 µm, and a thick choroid is defined by a thickness of more than 390 µm.

PNV is typically presented in OCT as CNV with choroidal thickening and missing drusen. Very typical indicators are irregular and very flat PEDs. PNV can be converted to PCV disease.

The spectrum of pachychoroidal diseases includes four different disease groups: Pachychoroidal pigment epitheliopathy (PPE), central serous chorioretinopathy (CSCR), pachychoroidal neovasculopathy (PNV), polypoidal choroidal vasculopathy (PCV). One disease may pass into another. PPE shows small focal RPE detachments, no drusen, and no subretinal fluid and may be a precursor of CSCR. In summary, PPE shows choroidal thickening, thinning in choriocapillaris and changes in RPE [29].

RAP

The RAP lesion described by Yannuzzi 2001 [30] is a specific clinical form of neovascularization in AMD. Neovascularization originates from the outer retinal layer and grows towards RPE (type 3 CNV). RAP-CNV does not respond properly to anti-VEGF treatment.

Hyperreflexive focus on drusen in the outer retinal layer is probably a precursor of the RAP lesion. The identification of precursor signs in SD-OCT is possible by using a B-Scan OCT

with high sample density and eye tracking mode. It may take about 21 months to complete progression from precursor to RAP level [31].

RPE Thickening Due to Deposits

Pattern Dystrophy: APMD (Adult Onset Pseudovitelliform Macular Dystrophy)

Pattern dystrophies show a high variety of macular phenomena (butterfly-shaped macular dystrophy, APMD). In funduscopy, a yellow or orange elevation of the fovea in the OCT correlates with a disorder at the RPE level. In pseudovitelliform macular dystrophy (APMD) in adults, moderate to highly reflective material lies beneath the sensory retina and above the RPE [32]. OCT shows a dome-shaped, subretinal, homogeneous hyporeflective layer between the RPE/fracture membrane and the ellipsoid zone of the photoreceptors (Fig. 12.16a, b).

The lesion may also resemble large serous drusen. But APMD occurs with a single foveal yellowish lesion and AMD shows drusen in larger numbers. Discrimination is also possible in the OCT. Serous drusen in OCT show an RPE detachment with an optically empty lumen or a medium reflective filling of the PED (Fig. 12.16a, b). In contrast, APMD shows an increase of a mean reflective convex area above the RPE. This image simulates a CNV in OCT, sometimes also in funduscopy. But unlike CNV, VA is much better and typically OCT shows no subretinal fluid, intraretinal cysts, or hemorrhage.

In about 12% after 6 years, CNV can occur as a rare complication of APMD. In FLA, the drusenoid material leads to staining that can be confused with CNV. The diagnosis is usually obvious, but in difficult cases follow-up of the disease, VA, OCT (fluid accumulation?) and FLA (multimodal imaging) leads to the correct diagnosis.

OCT-A is able to clearly show the presence of CNV, which is hardly visible in the FLA due

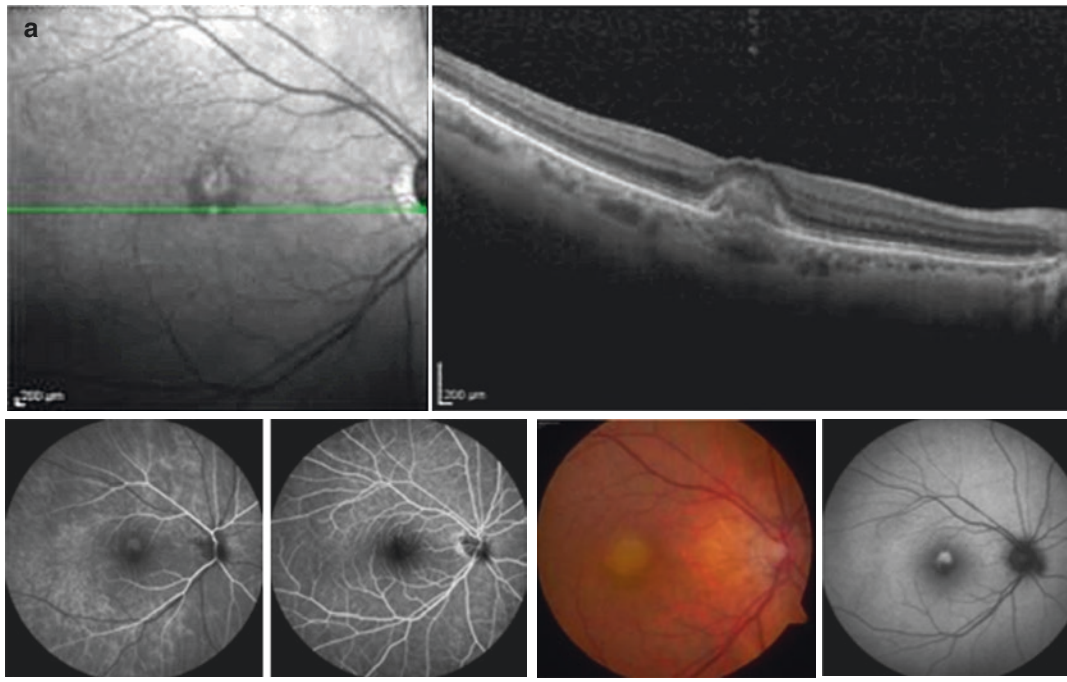

Fig. 12.16 (**a**) VA of both eyes 1.0. OCT shows convex thickening in OD as in CNV, but never accompanied by edema or subretinal fluid. The fundus image shows a typical yellow spot of the macula, also in autofluorescence (AF) a white spot without lipofuscin. The FLA below typically shows no leakage, only slight staining of the lipofuscin deposit. (**b**) SD-OCT shows a convex elevation above RPE-BM without fluid accumulation. The underlying RPE/BM layer is hardly visible under the vitelliform deposit

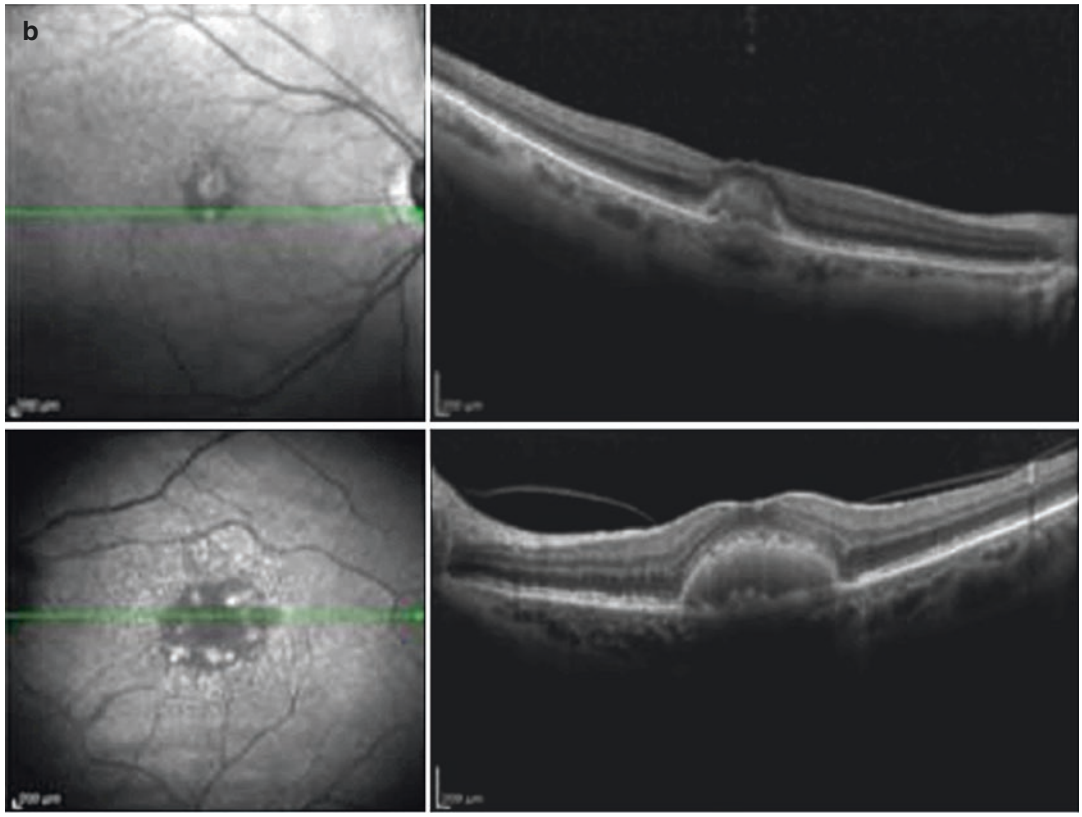

Fig. 12.16 (continued)

to blocking phenomena of vitelliform deposit. Vascular abnormalities in the OCT-A are nonspecific in the superficial and deep capillary plexus. The most important advantage of OCT-A in APMD is the detection of the underlying CNV, which is better detected in OCT-A than in FLA [33].

Best's Disease (Vitelliform Disease)

Best's disease is an autosomal dominant dystrophy of the macula. In vitelliform stage 2 of Best's disease, the subretinal material is homogeneous and hyperreflective. In pseudohypopyon stage 3 there is a homogeneous hyporeflective layer above the hyperreflective layer. This can be misunderstood as subretinal fluid after CNV. The "crumbled egg" stage 4 shows RPE atrophy and hypertrophy (Fig. 12.17). Stage 5, finally, shows a macular scar.

Best's disease very impressively shows that OCT is an image of reflectivity and not histology. The OCT image shows significant distortion of the normal layer structure of the retina.

In OCT, no structure is visible at the photoreceptor and RPE levels, but the VA is 1.0 (Fig. 12.17). Therefore, photoreceptors must be present but are not visible in OCT. The light beam of the OCT is backscattered by the vitelliform deposit and therefore does not reach the photoreceptors and the RPE/BM complex PED. This area does not seem to be absent, but it shows an artifact of the reflectivity image by the OCT.

It is of great interest at which layer vitelliform deposits accumulate. The average thickness of the foveal RPE/BM layer is significantly reduced in Best's disease (all stages) compared to healthy subjects, but not outside the fovea. The vitelliform deposit is most likely located within the interdigitation zone or the RPE/BM complex. It is possible that RPE may continue to form a preserved photoreceptor-RPE complex that provides essential nutrients to the photoreceptors and in turn helps patients maintain better than expected VA for years [34].

Histology shows that the vitelliform deposit between Bruch's membrane and RPE accumulates in the fovea. This material appeared to be derived from degenerating pigment epithelial cells and contained only a few intact lipofuscin granules. Loss of the foveal photoreceptor also occurred above the lesion [35].

The outer retinal layers remains in stage 1, but an interruption can be seen in stage 2–5. The vitelliform material is always found in stage 2 and 3, predominantly in stage 4 and rarely in stage 5. Neurosensory detachment occurred in stages 3 and 4. The more the vitelliform deposit decreased with the progressive development of Best's disease, the more the outer retinal layers were interrupted in the advanced stage [36].

RPE Atrophy

Geographical Atrophy (GA)

The atrophy of RPE is based on two or three criteria in a range of >125 µm: increased signal transmission through the choroid (choroidal

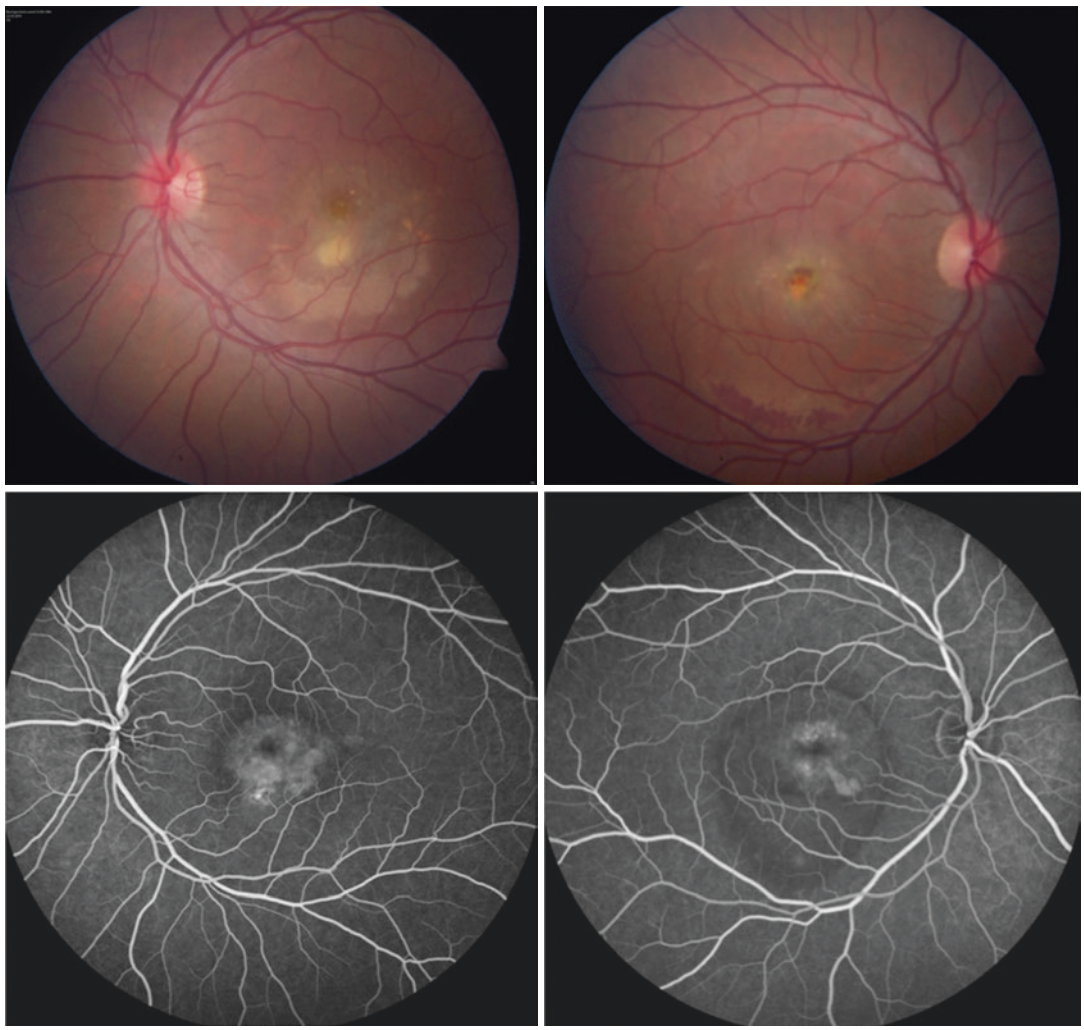

Fig. 12.17 24-year-old male patient, VA 0.8 and 1.0 with Best's disease. The colored fundus image shows typical intermediate morbus Best's (upper line). The FLA of the Best's disease, a patchy, mild hyperfluorescence is visible that corresponds to staining of the vitelliform deposits (center). In SD-OCT, extensive subretinal detachment of the macula over the attached RPE/BM layer (bottom)

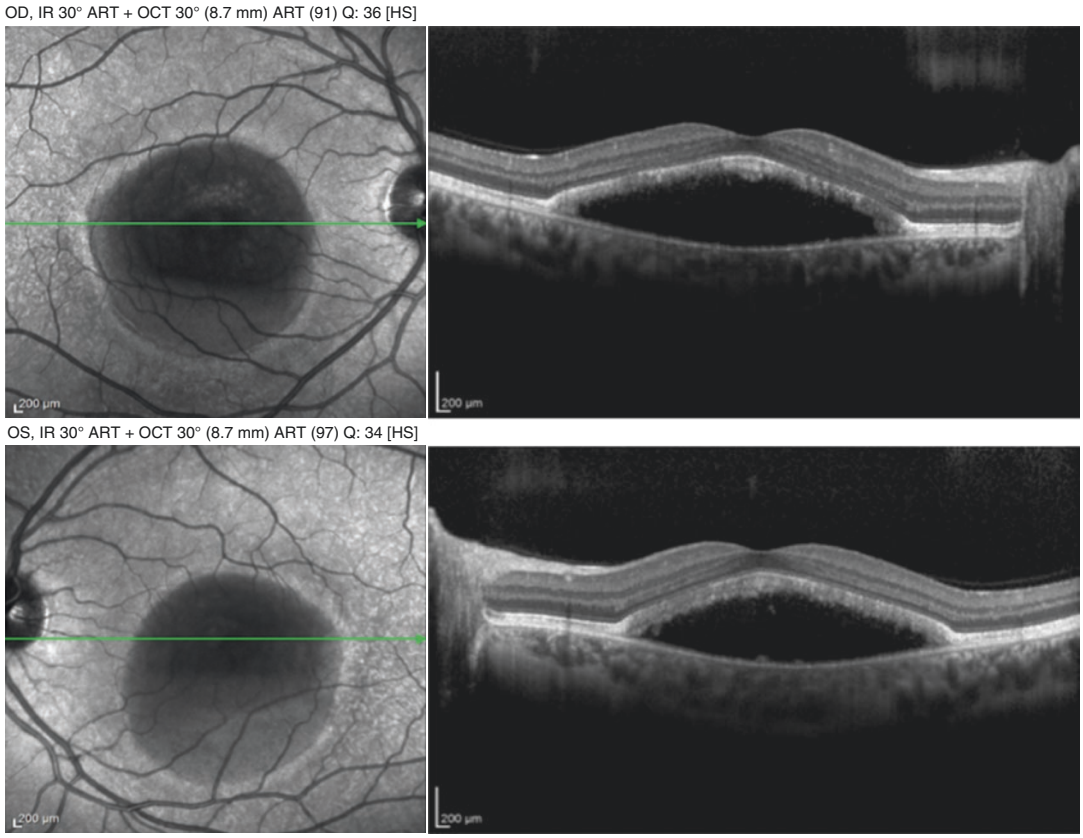

Fig. 12.17 (continued)

hypertransmission), attenuation of the RPE band and loss of the outer retinal layers [19].

GA is a form of dry AMD and occurs with increasing atrophy of the overlying RPE. SD-OCT results in a large-area deficiency of the RPE BM layer with subsequent reverse shadowing in SD-OCT. Due to the absence of the highly reflective RPE layer, the light can penetrate deeper layers (Fig. 12.18).

A broad spectrum of morphological changes in SD-OCT can be found in the GA, both in the surrounding area and in the atrophic region. These changes may represent different disease stages or different molecular heterogeneity [10].

Further longitudinal studies must demonstrate the prognostic effect of these morphological changes. The quantitative indicators for the progression of the disease from early AMD to advanced AMD (within 2 years) were the outer retinal thickness, the drusen area and the hyperreflective focus. Predictive hallmarks for CNV were drusen-centered, while hallmarks for GA were associated with neurosensory retina and age, using artificial intelligence [37].

The magnitude of the RPE visible in OCT and the defects of the photoreceptor in GA lesions differ significantly. These include the outer segments of the photoreceptor that remain in the absence of RPE cells and vice versa. These results are also important for understanding pathogenesis and treatment development [38].

The perfusion of choriocapillaris was significantly reduced adjacent to GA (AMD) measured with OCT-A. Choriocapillaris hypoperfusion was correlated with a loss of the cone photoreceptor. This suggests that reduced choriocapillaris perfusion contributes to the development of GA [39].

Choriocapillaris flow impairment around GA correlates with the annual growth rate of GA

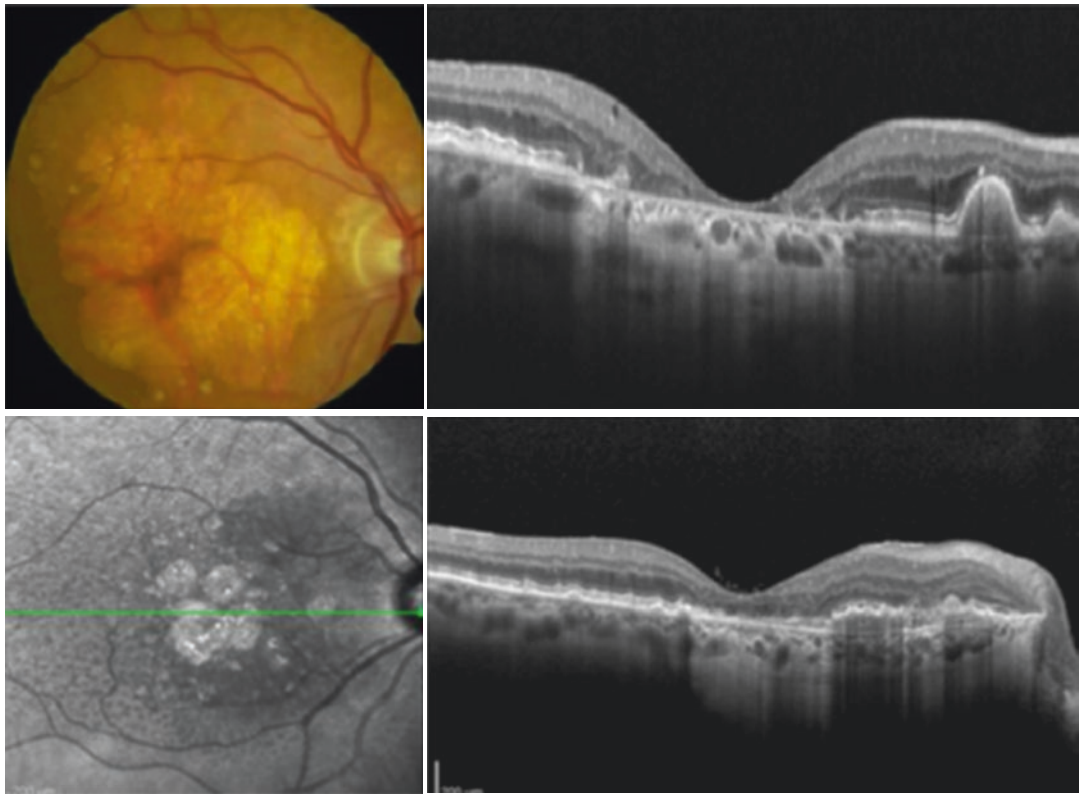

Fig. 12.18 The fundus image shows a typical GA. In OCT, the atrophy of the RPE is subfoveal and additionally large drusen are visible. The OCT identifies typical focal light enhancement as there is no highly reflective RPE

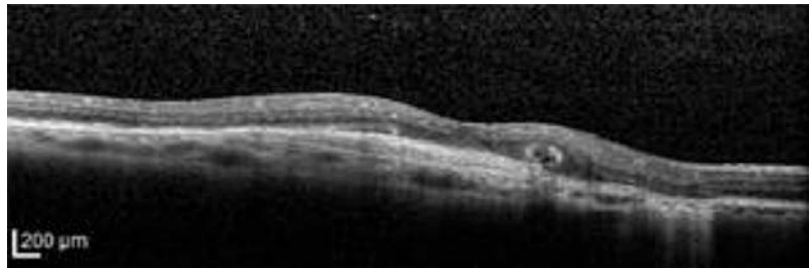

Fig. 12.19 An outer retinal tubulation is identified by OCT over the RPE-BM complex within the outer retinal layers. It is suspected that degenerating photoreceptors are arranged in a circle (circular hyperreflectivity in OCT)

expansion. This shows a useful parameter for prognostic surrogate in patients with GA [40].

A special condition in GA is represented by the outer retinal tubulation (ORT) (Fig. 12.19). It is presumed that degenerating photoreceptors become arranged circular. Individual RPE cells are found in the lumen of the ORT. The ORT must be differentiated from intraretinal cyst formation because unnecessary treatment may possibly be prompted [41].

Stargardt's Disease and Fundus Flavimaculatus

The abnormal deposits in the fundus flavimaculatus can be located on the RPE layer confirmed by OCT. In Stargardt's disease, atrophy of the outer

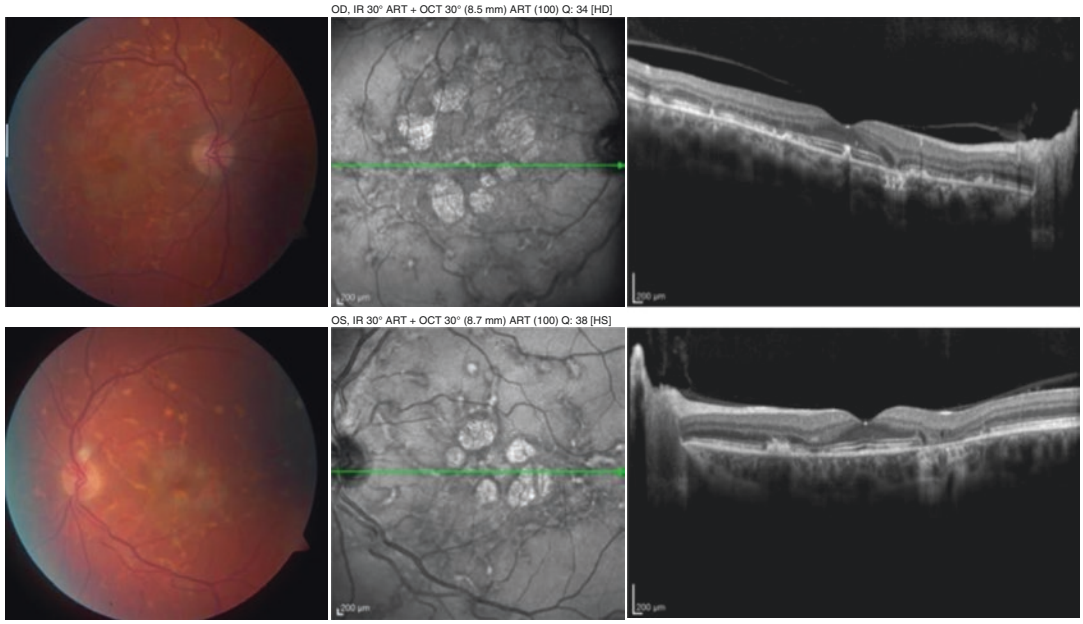

Fig. 12.20 In case of Stargardt's disease with fundus flavimaculatus VA both eyes 1.0. Left: The funduscopic white lesions show focal atrophy of the RPE in OCT. The abnormal deposits in the fundus flavimaculatus can be localized on the RPE layer as focal thickening confirmed by OCT

retinal layers and the RPE can also be observed. Stargardt's disease with fundus flavimaculatus shows focal thickening and atrophy of the RPE simultaneously (Fig. 12.20).

In SD-OCT, the area of ellipsoid zone loss is more reliable than the RPE [42] for monitoring the course of disease in Stargardt's disease.

The choroidal flow signal with OCT-A differs in RPE atrophy in late onset Stargardt's disease and AMD. This choroidal different perfusion may implicate a different pathogenesis of RPE atrophy in both diseases [43].

Choroideremia

A severe loss of RPE in choreoideremic diseases increases the light transmission from OCT to choroid and sclera. The sensory retina appears to lie on the choroid/choriocapillary. Without the highly reflective RPE, deeper penetration into the choroid and sclera is possible.

Choriocapillaris and choroid appear to be almost completely absent (Fig. 12.21). The RPE layer and a very thin choroid lie directly adjacent to the thick sclera. Due to the lack of highly reflective RPE and choroidal vascular supply, the sclera is clearly visible in this situation of choroideremia (Fig. 12.21).

Quantification of the RPE layer and ellipsoid zone on OCT images is highly reproducible and therefore suitable for clinical studies and follow-up [44]. In OCT-A, early vascular abnormalities in the inner retinal layers and choriocapillaris can be observed. In addition, a reduced vascular flow was detectable in preserved macular RPE. OCT-A is useful to detect the vascular situation early in choroideremia [45].

The loss of RPE after inflammation or infectious diseases may lead to the same appearance in OCT, e.g. serpiginous choroiditis, toxoplasmic chorioretinitis, birdshot chorioretinopathy.

Secondary Toxic RPE Damage

Solar/Laser Retinopathy

Looking into the sun or high-energy lasers (such as industrial lasers or non-approved laser pointers) can cause severe retinal damage. The absorption of the laser radiation in visible light (often red 670 nm and green 532 nm) occurs mainly

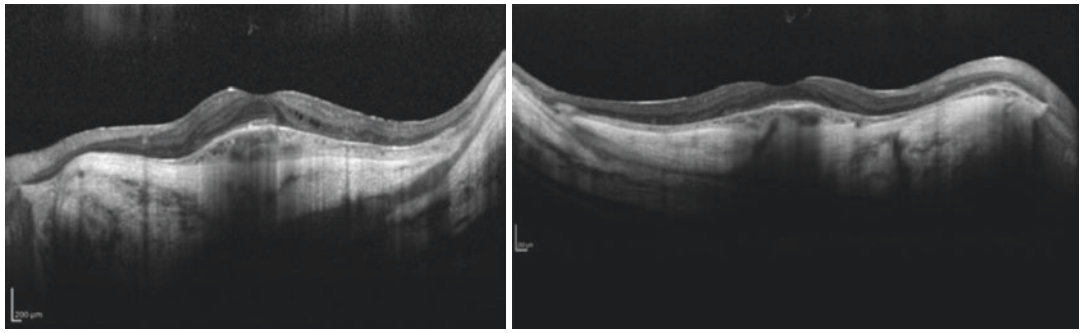

Fig. 12.21 An OCT of choroideremia shows the absence of a highly reflective RPE layer and choriocapillary, but very deep insight into the choroid and sclera

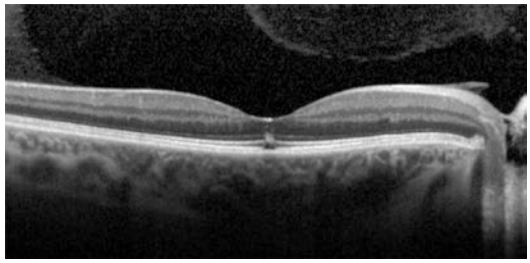

Fig. 12.22 Spectralis OCT image of a 34-year-old woman (VA 0.6) observing a partial solar eclipse without special protective glasses. OCT shows a hyporeflective area subfoveally and a disorder of the photoreceptors

in the outer layers of the retina; the RPE is typically spared (Fig. 12.22). This results in damage that leads to degeneration of the photoreceptors. Sun arc injuries occur in OCT as focal loss of the outer retina and the IS-OS/ellipsoid layer, leaving a small hyporeflective rectangular cavity. Complications of laser exposure include retinal hemorrhage, CNV and chronic macular edema [46, 47]. Histological studies have localized the damage of the outer segments of the foveal photoreceptor and the RPE.

Poppers Maculopathy

Poppers (isopropyl nitrate) are inhaled to give people a brief period of exhilaration. They contain liquid nitrogen chemicals which cause a flush of arterial dilatation. Poppers have recently been used to treat angina pectoris and can affect the macula by causing macular degeneration at an early age at the level of RPE. Poppers maculopathy may occur and presents as vitelliform lesions of the central macula (Fig. 12.23). The pathomechanism is still unclear but may be associated with modulated photoreceptor metabolism due to increased blood NO concentrations and vasodilatation. A vitelliform lesion in OCT of the fovea is shown above the RPE (Fig. 12.23). In SD-OCT, a blurred defect of the outer elements of the photoreceptors can be found. The RPE is slightly affected and appears blurred.

Summary and Future Developments

SD-OCT of the RPE has developed so far that we can now image the retinal microstructure [20]. SD-OCT technology has been successfully implemented in modern OCT systems and enables us to provide high-resolution imaging of the retina in vivo. This has greatly improved our understanding of RPE anatomy and function as well as changes in different pathological units. However, we must bear in mind that OCT is based on reflectivity, so association with histological data must be made carefully. The evaluation of AMD, a disease whose pathogenesis is in the RPE and adjacent structures, has greatly benefited from the introduction of SD-OCT. With the continuing rapid development of new imaging technologies, it is likely that OCT will provide further insights into the pathophysiology and treatment of retinal diseases.

The following developments contribute to the implementation and increasing importance

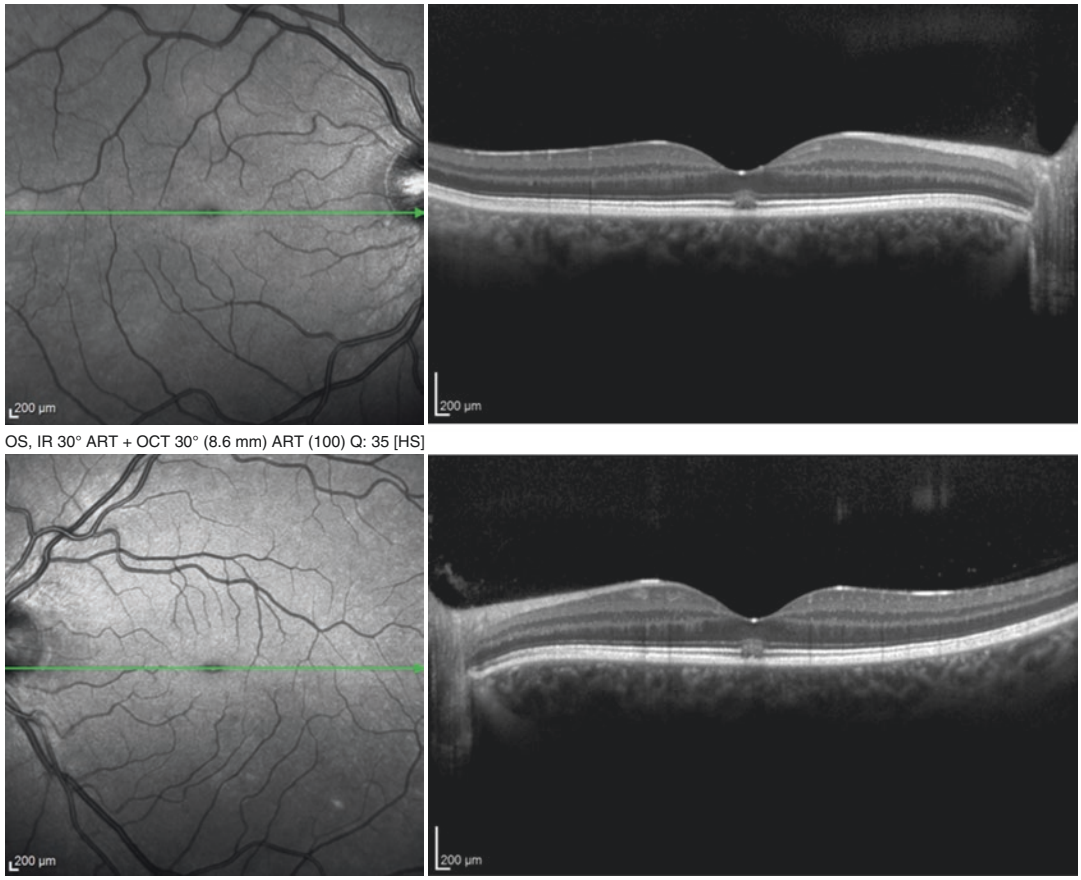

Fig. 12.23 The use of poppers leads to a vitelliform lesion in OCT and a visual deterioration (VA 0.3). The outer retinal layers (photoreceptors) and the RPE layer are affected and blurred

of OCT and OCT-A: Development of higher resolution, faster scan acquisition (software), automated segmentation and OCT angiography. In macular diseases, especially AMD, structural changes can be visualized in a large image analysis and can help in predicting the course of the disease and the prognosis. The development of potential biomarkers is possible. The higher the resolution and the individual layers of the retina can be visualized, the more predictive biomarkers can be developed.

Based on the extensive availability of OCT data, self-learning artificial intelligence (AI) may in the future be able to identify and examine patients and healthy volunteers with macular disease [37]. AI may play an important role for outpatients in the future, although there are limitations in the use of AI only for follow-up [48]. But it may be an option in the future for AI to help study the diseased and healthy population through telemedicine or even an app on the smartphone. The screening values can then lead to consultation with a specialist to confirm a suspected diagnosis.

References

1. Huang D, Swanson E, Lin C, Schuman J, Stinson W, Chang W, et al. Optical coherence tomography. Science. 1991;254:1178–81.
2. Swanson EA, Izatt JA, Hee MR, Huang D, Lin CP, Schuman JS, et al. In vivo retinal imaging by optical coherence tomography. Opt Lett. 1993;18:1864–6.
3. Ash C, Town G, Clement M. Confirmation of spectral jitter: a measured shift in the spectral distribution of intense pulsed light systems using a time-resolved spectrometer during exposure and increased fluence. J Med Eng Technol. 2010;34:97–107.

4. N'soukpoé-Kossi CN, Leblanc RM. Absorption and photoacoustic spectroscopies of lutein and zeaxanthin Langmuir–Blodgett films in connection with the Haidinger's brushes. Can J Chem. 1988;66:1459–66.
5. Prahl S. Optical absorption of indocyanine green (ICG). 2018. https://omlc.org/spectra/icg/
6. Coscas GJ, Lupidi M, Coscas F, Cagini C, Souied EH. Optical coherence tomography angiography versus traditional multimodal imaging in assessing the activity of exudative age-related macular degeneration: a new diagnostic challenge. Retina. 2015;35:2219–28.
7. Lee JM, Park SC. The argument for swept-source OCT. Ophthalmol Manag. 2016;20:20–2.
8. Karampelas M, Sim DA, Keane PA. Spectral-domain OCT of the RPE. Retin Physician. 2014;11:53–9.
9. Runkle AP, Kaiser PK, Srivastava SK, Schachat AP, Reese JL, Ehlers JP. OCT angiography and ellipsoid zone mapping of macular telangiectasia type 2 from the AVATAR study. Invest Opthalmol Vis Sci. 2017;58:3683.
10. Fleckenstein M, Issa PC, Helb H-M, Schmitz-Valckenberg S, Finger RP, Scholl HPN, et al. High-resolution spectral domain-OCT imaging in geographic atrophy associated with age-related macular degeneration. Invest Opthalmol Vis Sci. 2008;49:4137.
11. Keane PA, Patel PJ, Liakopoulos S, Heussen FM, Sadda SR, Tufail A. Evaluation of age-related macular degeneration with optical coherence tomography. Surv Ophthalmol. 2012;57:389–414.
12. Schmitz-Valckenberg S, Steinberg JS, Fleckenstein M, Visvalingam S, Brinkmann CK, Holz FG. Combined confocal scanning laser ophthalmoscopy and spectral-domain optical coherence tomography imaging of reticular drusen associated with age-related macular degeneration. Ophthalmology. 2010;117:1169–76.
13. Moore DJ, Clover GM. The effect of age on the macromolecular permeability of human Bruch's membrane. Invest Ophthalmol Vis Sci. 2001;42:2970–5.
14. Balaratnasingam C, Messinger JD, Sloan KR, Yannuzzi LA, Freund KB, Curcio CA. Histologic and optical coherence tomographic correlates in drusenoid pigment epithelium detachment in age-related macular degeneration. Ophthalmology. 2017;124:644–56.
15. Curcio CA, Zanzottera EC, Ach T, Balaratnasingam C, Freund KB. Activated retinal pigment epithelium, an optical coherence tomography biomarker for progression in age-related macular degeneration. Invest Ophthalmol Vis Sci. 2017;58:BIO211–26.
16. De Salvo G, Vaz-Pereira S, Keane PA, Tufail A, Liew G. Sensitivity and specificity of spectral-domain optical coherence tomography in detecting idiopathic polypoidal choroidal vasculopathy. Am J Ophthalmol. 2014;158:1228–1238.e1.
17. Feucht N, Maier M, Lohmann CP, Reznicek L. OCT angiography findings in acute central serous chorioretinopathy. Ophthalmic Surg Lasers Imaging Retina. 2016;47:322–7.
18. Ferris FL, Wilkinson CP, Bird A, Chakravarthy U, Chew E, Csaky K, et al. Clinical classification of age-related macular degeneration. Ophthalmology. 2013;120:844–51.
19. Gattoussi S, Buitendijk GHS, Peto T, Leung I, Schmitz-Valckenberg S, Oishi A, et al. The European Eye Epidemiology spectral-domain optical coherence tomography classification of macular diseases for epidemiological studies. Acta Ophthalmol. 2019;97:364–71.
20. Keane PA, Karampelas M, Sim DA, Sadda SR, Tufail A, Sen HN, et al. Objective measurement of vitreous inflammation using optical coherence tomography. Ophthalmology. 2014;121:1706–14.
21. Querques G, Georges A, Ben Moussa N, Sterkers M, Souied EH. Appearance of regressing drusen on optical coherence tomography in age-related macular degeneration. Ophthalmology. 2014;121:173–9.
22. Klein R, Klein BEK, Tomany SC, Meuer SM, Huang G-H. Ten-year incidence and progression of age-related maculopathy: the Beaver Dam Eye Study. Ophthalmology. 2002;109:1767–79.
23. Sohrab MA, Smith RT, Salehi-Had H, Sadda SR, Fawzi AA. Image registration and multimodal imaging of reticular pseudodrusen. Invest Opthalmol Vis Sci. 2011;52:5743.
24. Regatieri CV, Branchini L, Duker JS. The role of spectral-domain OCT in the diagnosis and management of neovascular age-related macular degeneration. Ophthalmic Surg Lasers Imaging. 2011;42:S56–66.
25. Roberts PK, Baumann B, Schlanitz FG, Sacu S, Bolz M, Pircher M, et al. Retinal pigment epithelial features indicative of neovascular progression in age-related macular degeneration. Br J Ophthalmol. 2017;101:1361–6.
26. Farecki M-L, Gutfleisch M, Faatz H, Rothaus K, Heimes B, Spital G, et al. Characteristics of type 1 and 2 CNV in exudative AMD in OCT-angiography. Graefes Arch Clin Exp Ophthalmol. 2017;255:913–21.
27. Corvi F, Cozzi M, Barbolini E, Nizza D, Belotti M, Staurenghi G, et al. Comparison between several optical coherence tomography angiography devices and indocyanine green angiography of choroidal neovascularization. Retina. 2019.
28. Told R, Sacu S, Hecht A, Baratsits M, Eibenberger K, Kroh ME, et al. Comparison of SD-optical coherence tomography angiography and indocyanine green angiography in type 1 and 2 neovascular age-related macular degeneration. Invest Opthalmol Vis Sci. 2018;59:2393.
29. Akkaya S. Spectrum of pachychoroid diseases. Int Ophthalmol. 2018;38:2239–46.
30. Yannuzzi LA, Negrão S, Iida T, Carvalho C, Rodriguez-Coleman H, Slakter J, et al. Retinal angiomatous proliferation in age-related macular degeneration. Retina Phila Pa. 2001;21:416–34.
31. Öztaş Z, Menteş J. Retinal angiomatous proliferation: multimodal imaging characteristics and follow-up with eye-tracked spectral domain optical coherence

tomography of precursor lesions. Türk Oftalmol Derg. 2018;48:66–9.
32. Benhamou N, Souied EH, Zolf R, Coscas F, Coscas G, Soubrane G. Adult-onset foveomacular vitelliform dystrophy: a study by optical coherence tomography. Am J Ophthalmol. 2003;135:362–7.
33. Gass JD, Jallow S, Davis B. Adult vitelliform macular detachment occurring in patients with basal laminar drusen. Am J Ophthalmol. 1985;99:445–59.
34. Qian CX, Charran D, Strong CR, Steffens TJ, Jayasundera T, Heckenlively JR. Optical coherence tomography examination of the retinal pigment epithelium in best vitelliform macular dystrophy. Ophthalmology. 2017;124:456–63.
35. O'Gorman S, Flaherty WA, Fishman GA, Berson EL. Histopathologic findings in Best's vitelliform macular dystrophy. Arch Ophthalmol. 1988;106:1261–8.
36. Battaglia Parodi M, Iacono P, Romano F, Bolognesi G, Fasce F, Bandello F. Optical coherence tomography in best vitelliform macular dystrophy. Eur J Ophthalmol. 2017;27:201–4.
37. Schmidt-Erfurth U, Klimscha S, Waldstein SM, Bogunović H. A view of the current and future role of optical coherence tomography in the management of age-related macular degeneration. Eye. 2017;31:26–44.
38. Qu J, Velaga SB, Hariri AH, Nittala MG, Sadda S. Classification and quantitative analysis of geographic atrophy junctional zone using spectral domain optical coherence tomography. Retina. 2018;38:1456–63.
39. Qin J, Rinella N, Zhang Q, Zhou H, Wong J, Deiner M, et al. OCT angiography and cone photoreceptor imaging in geographic atrophy. Invest Opthalmol Vis Sci. 2018;59:5985–92.
40. Nassisi M, Baghdasaryan E, Borrelli E, Ip M, Sadda SR. Choriocapillaris flow impairment surrounding geographic atrophy correlates with disease progression. PLoS One. 2019;14:e0212563.
41. Zweifel SA. Outer retinal tubulation: a novel optical coherence tomography finding. Arch Ophthalmol. 2009;127:1596.
42. Cai CX, Light JG, Handa JT. Quantifying the rate of ellipsoid zone loss in Stargardt disease. Am J Ophthalmol. 2018;186:1–9.
43. Müller PL, Pfau M, Möller PT, Nadal J, Schmid M, Lindner M, et al. Choroidal flow signal in late-onset Stargardt disease and age-related macular degeneration: an OCT-angiography study. Invest Opthalmol Vis Sci. 2018;59:AMD122.
44. Hariri AH, Velaga SB, Girach A, Ip MS, Le PV, Lam BL, et al. Measurement and reproducibility of preserved ellipsoid zone area and preserved retinal pigment epithelium area in eyes with choroideremia. Am J Ophthalmol. 2017;179:110–7.
45. Murro V, Mucciolo DP, Giorgio D, Sodi A, Passerini I, Virgili G, et al. Optical coherence tomography angiography (OCT-A) in young choroideremia (CHM) patients. Ophthalmic Genet. 2019;40(3):201–6.
46. Fujinami K, Yokoi T, Hiraoka M, Nishina S, Azuma N. Choroidal neovascularization in a child following laser pointer-induced macular injury. Jpn J Ophthalmol. 2010;54:631–3.
47. Wyrsch S, Baenninger PB, Schmid MK. Retinal injuries from a handheld laser pointer. N Engl J Med. 2010;363:1089–91.
48. Harkness Eye Institute, Columbia University, New York, United States, Kapoor R, Whigham BT, Al-Aswad LA. Artificial intelligence and optical coherence tomography imaging. Asia-Pac J Ophthalmol [Internet] 2019 [cited 2019 Jun 11]. http://www.apjo.org/Apjo/pdf/id/654.html.